THE LORENZ ENERGY CYCLE OF THE GLOBAL ATMOSPHERE DURING THE PAST 35 YEARS (1979-2013)

A Dissertation Presented to

the Faculty of the Department of Physics

University of Houston

In Partial Fulfillment

of the Requirements for the Degree

Doctor of Philosophy

By

Yefeng Pan

December 2015

THE LORENZ ENERGY CYCLE OF THE GLOBAL ATMOSPHERE DURING THE PAST 35 YEARS (1979-2013)

_____

Yefeng Pan

APPROVED:

_____

Dr. Liming Li, Chairman

_____

Dr. Gemunu Gunaratne

_____

Dr. Donna Stokes

_____

Dr. Wu-Pei Su

_____

Dr. Xun Jiang

_____

Dean, College of Natural Sciences and Mathematics

Acknowledgments

I would like to express my sincerest gratitude to my advisors, Dr. Liming Li and Dr. Xun Jiang, for their guidance, encouragement, and continuous support during the years of my Ph.D. study and research. Their patience, motivation, and enthusiasm for their research inspired me to perform to the utmost of my potential to the scientific community. Their guidance has benefitted me during my graduate studies and will continue to a play an important part throughout my future endeavors.

Besides my advisors, I would like to thank the rest of my committee members: Dr. Gemunu Gunaratne, Dr. Donna Stokes and Dr. Wu-Pei Su, for their helpful insights, comments, and encouragement, and also for the stimulating questions, which motivated me to widen my research knowledge from various perspectives.

I would also like to thank Dr. Danie Liang who helped me download extensive data, which saved me a lot of time and made my research easier. I would like to thank Jingqian Wang whose research materials benefited me a lot. I also want to thank my fellow labmates: Justin Trammell, James Trammell, Angela Kao, Joseph Hernandez, Abbie Corbett, Jie Liu, Joseph Hernandez, and Aaron Studwell. They provided support and help during my graduate career. I am very grateful to Jennifer Chin-Davis and Naomi Haynes for their help.

I want thank to Dr. Qiuzhao Dong, who provided me with an intern opportunity, in which I attained additional experience and enhanced my coding skills.

Especially, I would like to thank Joseph Hernandez who helped me revise my dissertation.

Last but not least, I would like to thank my parents and all of my friends who supported and encouraged me during my graduate years.

THE LORENZ ENERGY CYCLE OF THE GLOBAL ATMOSPHERE DURING THE PAST 35 YEARS (1979-2013)

An Abstract of a Dissertation

Presented to

the Faculty of the Department of Physics

University of Houston

In Partial Fulfillment

of the Requirements for the Degree

Doctor of Philosophy

By

Yefeng Pan

December 2015

Abstract

The Lorenz energy cycle (Lorenz 1955) describes how the solar heating generates potential energy that can be converted into kinetic energy to drive Earth's atmospheric system. Therefore, the studies of the Lorenz energy cycle can help us understand the atmospheric system from a unique energy perspective.

Based on two best global meteorological datasets, we systematically study the Lorenz energy cycle of the global atmosphere during the modern satellite era (1979-2013). Our analyses provide the most reliable characteristics of the Lorenz energy cycle of the global atmosphere. The mean state of the 35-year Lorenz energy cycle generates the best global picture of the Lorenz energy cycle.

Our analyses also reveal important temporal characteristics of the Lorenz energy cycle of the global atmosphere. Significant positive trends are shown in both the eddy available potential energy (P_E) and the eddy kinetic energy (K_E) especially in the Southern Hemisphere, which are mainly due to the increasing storm activities over the Southern Ocean storm track areas. At the same time, a negative trend is seen in the mean available potential energy (P_M) especially around the North Pole near the surface, which is probably related to the inhomogeneous global warming. As a result, the total mechanical energy does not show any significant trend during the past 35 years, which suggests that the climate system remains close to a dynamical balance. Our analyses also suggest positive trends in all conversion rates and in the dissipation of kinetic energy,

which implies that the efficiency of the global atmosphere as a heat engine increased during the modern satellite era.

The statistical characteristics of the Lorenz energy cycle revealed in our analyses will provide a powerful tool to validate and develop the atmospheric and climate models. The temporal characteristic of the Lorenz energy cycle will also benefit the monitoring and predicting of climate change, for the atmospheric energetics are an important component of climate system of Earth.

Table of Contents

1 Introduction

1.1 Basic Concepts

Atmospheric energetics is an important branch of atmospheric science (Peixoto and Oort 1992). There are different energy components (e.g., latent heat, sensitive heat, radiation, and mechanical energies) in the atmospheric system. Atmospheric energetics describes the roles and conversion/transportation of these energy components and how they affect the atmospheric system. Therefore, the studies of the atmospheric energetics provide us a powerful tool to diagnose the energy flows in the atmospheric system and hence help us better understand Earth's atmospheric system and the corresponding weather and climate.

The atmospheric energetics can be explored from different perspectives. The radiant energy budget between the incoming solar radiation and the reflections/emissions of the different elements of Earth system (e.g., atmosphere, ocean, and land) is generally displayed in the format of flow diagrams (e.g., Hartmann (1994)). Such a flow diagram is shown in Figure 1.1. The diagram shows how much the total radiant energy comes from the Sun (i.e., solar constant), how much the solar radiant energy is reflected to space at

the top of the atmosphere, and how much the solar radiant energy is absorbed by Earth's system. The Earth's system emits roughly the same amount energy as the absorbed energy, so it is in a quasi-equilibrium state. In addition to the radiant energy balance at the top of the atmosphere, the transfer and distribution of radiant energy within the atmospheric systems modify the thermal structure to generate available potential energy. The available potential energy can be further converted into kinetic energy to drive atmospheric circulation and the related weather and climate on Earth.

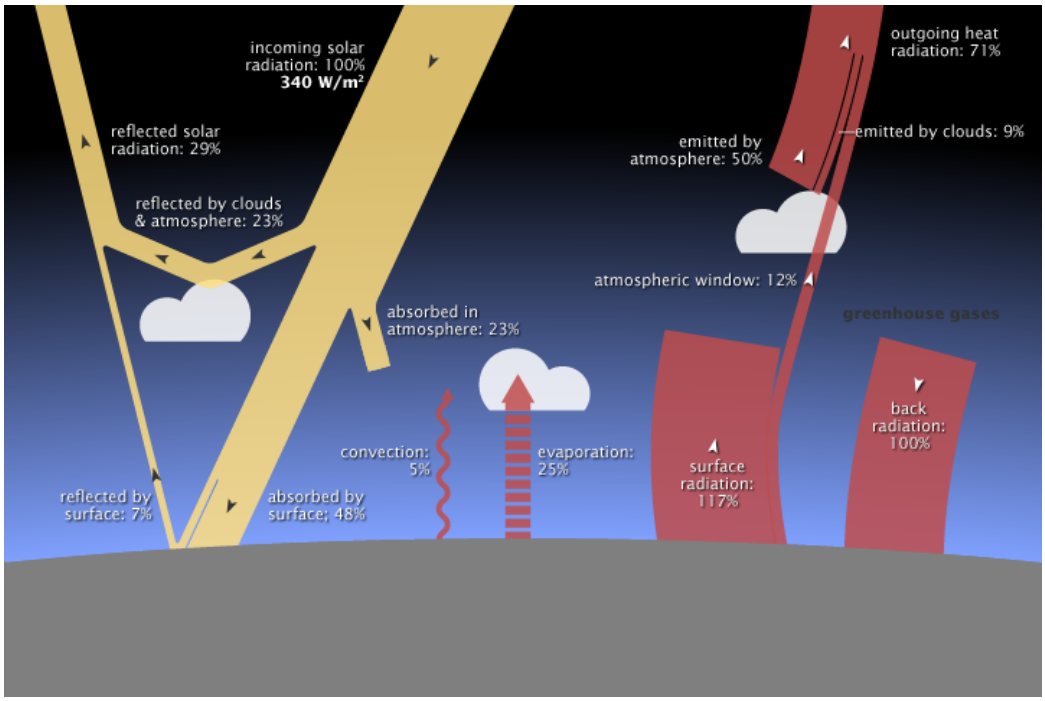

Figure 1.1 Radiant energy budget of Earth's system.

Therefore, the mechanical energy components (i.e., the potential energy and kinetic energy) play important roles in the atmospheric system of Earth. This dissertation is mainly studying long-term atmospheric behaviors with emphasis on the mechanical energy components and their conversions. The mean states and temporal variations of mechanical energy components and conversion rates of the global atmosphere of Earth are investigated with the modern satellite-based meteorological datasets. It should be emphasized that the combination of the developed theoretical frame and the modern-time datasets make it possible to examine the long-term temporal variations of the global atmosphere for the first time.

The mechanical energy components, conversions among them, and generations/dissipations constitute the atmospheric energy cycle, which is first defined by Lorenz (1955) and also named as Lorenz energy cycle. A modern-time picture of the Lorenz energy cycle is shown in Fig. 1.2.

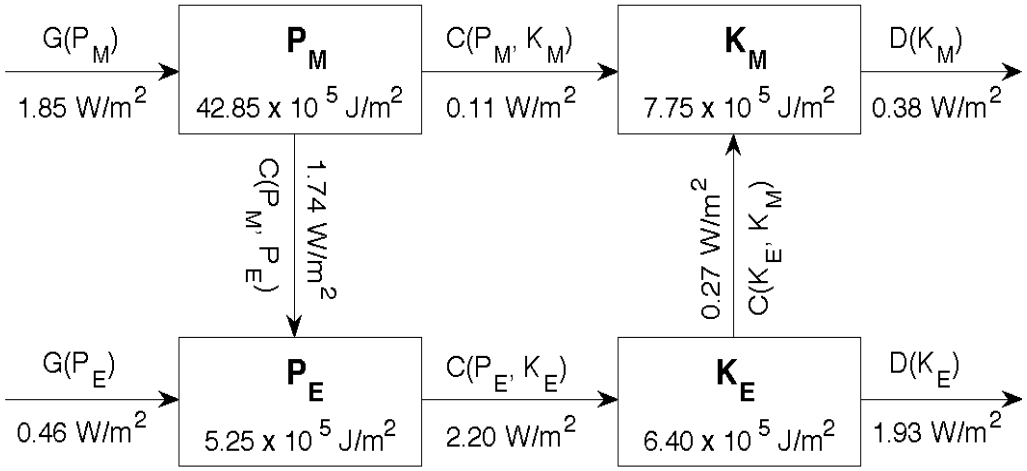

Figure 1.2 Lorenz energy cycle of the global atmosphere of Earth (modified from Li et al., 2007).

In the mixed space-time domain developed by Oort (1964), there are four energies, four conversion terms, two generation terms, and two dissipation terms in the Lorenz energy cycle. Here we introduce these energy components as below.

Mean Available Potential Energy (P_M): The theoretical part of the total potential energy of atmosphere, which can be converted into kinetic energy, is defined as the available potential energy. The mean available potential energy is the mean value of the available potential energy in both temporal and spatial domains.

Eddy Available Potential Energy (P_E):Variation of the available potential energy in both temporal (transient) and spatial (stationary) domains;

Mean Kinetic Energy (K_M): The kinetic energy is related the atmospheric motions (i.e., winds). The mean kinetic energy is the mean value of the kinetic energy in both temporal and spatial domains.

Eddy Kinetic Energy (K_E):Variation of the kinetic energy in both temporal (transient) and spatial (stationary) domains;

$C(P_M, P_E)$: Conversion from the mean available potential energy to the eddy available potential energy;

$C(P_E, K_E)$: Conversion from the eddy available potential energy to the eddy kinetic energy;

$C(K_E, K_M)$: Conversion from the eddy available kinetic energy to the mean kinetic energy;

$C(P_M, K_M)$: Conversion from the mean available potential energy to the mean kinetic energy;

$G(P_M)$: Generation of the mean available potential energy;

$G(P_E)$: Generation of the eddy available potential energy;

$D(K_M)$: Dissipation of the mean kinetic energy;

$D(K_E)$: Dissipation of the eddy kinetic energy.

1.2 Brief Review of the Studies of the Lorenz Energy Cycle

The first study of the mechanical energies of Earth's atmosphere were published ~ 100 years ago. Margules (1903) suggested the definition of total potential energy for the first time, which is the sum of the potential and internal energy. He defined the available potential energy as the maximum amount of total potential energy available for conversion into kinetic energy under any adiabatic redistribution of mass. In the study by Margules (1903), the available potential energy is defined for a fixed mass of atmosphere with a fixed region.

To generalize the definition of available potential energy, Lorenz (1955) introduced another definition for the whole atmosphere, in which the available potential energy was defined as the difference between the total potential energy of the whole atmosphere and the minimum of total potential energy, where the minimum of total potential energy would exist if the mass were redistributed under conservation of potential temperature in a horizontal stable stratification (Lorenz 1955). Using the definition of available potential energy and a common definition of kinetic energy in atmospheric system, Lorenz further introduced formula of energy components and energy conversions in wind velocity fields and temperature variations. With these energy terms and the conversions among them, an atmospheric energy cycle was constructed and

generally named as the Lorenz Energy Cycle. The framework developed by Lorenz (1955) was almost immediately utilized by Phillips (1956) in his classical work simulating the general circulation of the atmosphere in a two-level quasi-geostrophic model. Saltzman (1957) extended the equations in the wave-number domain by employing a Fourier transform so that different scales of motions, including planetary, synoptic, and mesoscale circulations, could be examined.

In 1964, Oort reformulated Lorenz's equations of atmospheric energetics in the mixed space and by using the primitive equations of motion (Oort 1964). Oort's formulation is the most-widely used in recent years because it does not make hydrostatic and geostrophic approximations. The other advantage of Oort's formulation is that it can discriminate between transient eddies (perturbations in time) and stationary eddies (perturbation in space). We will use Oort's formulation, which we have already used in a previous study (Li, Ingersoll et al. 2007, Li, Jiang et al. 2011) and discussed in detail in the chapter of "Theoretical Framework".

Based on the theoretical framework developed by Lorenz (1955) and Oort (1964), a series of studies has already been conducted. Considering that the observations before the satellite era (1979-2013) were mainly concentrated in the Northern Hemisphere, most of the previous studies (e.g., (Krueger, Winston et al. 1965, Wiinniel.A, Steinber.L et al. 1967, Oort and Peixoto 1974, Peixoto and Oort 1974, Oort and Peixoto 1976, Sheng and Hayashi 1990, Hu, Tawaye et al. 2004)). Based on a 10-year (1963-1973) rawinsonde dataset with a limitation of sparseness of stations in the Southern Hemisphere (SH) and

large data gaps at some stations, Oort (1983) conducted the first global study of the Lorenz energy cycle.

The most-important achievement of these previous studies is that they provided a basic picture of the Lorenz energy cycle of Earth's atmosphere. The datasets used in these previous studies basically do not include the satellite-based datasets. Therefore, there are serious limitations in the spatial resolution and coverage. Therefore, the energy components and conversion rates provided in these previous studies should be re-examined with the modern satellite-based meteorological datasets, which are the main objectives of our project.

1.3 Recent Progress in the Studies of the Lorenz Energy Cycle from Our Group

Little progress had been made in decades with the limitation of data coverage and precision in temporal and spatial domain. This was changed by release of two satellite-based datasets from the National Centers for Environmental Prediction — National Center for Atmospheric Research (NCEP-NCAR) and the European Center for Medium-Range Weather Forecasts (ECMWF) (Kalnay, Kanamitsu et al. 1996, Kanamitsu,

Ebisuzaki et al. 2002, Uppala 2002, Uppala, Kallberg et al. 2005). These modern datasets provide records of the atmospheric variables since 1979 (i.e., the beginning of modern satellite era) with the spatial coverage from pole to pole and the relatively high spatial resolutions.

A study (Li, Ingersoll et al. 2007) based on these datasets re-examined the mean state of the global atmospheric energy cycle. And it was the first time computing the energies and conversions with reliable satellite datasets with high precision for long-term and global coverage. This study calculated the mean state and spatial structure of four energy components (P_M, P_E, K_M and K_E) and four conversion rates ($C(P_M, P_E)$, $C(P_E, K_E)$, $C(K_E, K_M)$, and $C(P_M, K_M)$). This study also analyzed the energy and conversion terms in Hemispheres (Northern Hemisphere and Southern Hemisphere) and seasons (Spring, Summer, Fall and Winter). With the long-term and high-quality satellite datasets, the study (Li, Ingersoll et al. 2007) provided more robust picture of the Lorenz energy cycle of Earth atmosphere. In addition, the study corrected the wrong direction of conversion rate from the mean available energy to the mean kinetic energy ($C(P_M, K_M)$) presented in these previous studies.

One more study conducted by our research group (Li, Jiang et al. 2011) analyzed the Lorenz energy cycle of the global atmosphere in the El Nino and La Nina years. The analyses suggest ~ 1%–3% increase and 2%–3% decrease in the mean energies in the El Nino years and La Nina years, respectively. Our analyses further revealed that the

modified tropospheric temperature by the El Nino/La Nina events leads to the temporal variation of the mean atmospheric energies.

The recent studies from our group advanced our understanding of the Lorenz energy cycle and its relationship with the important climate events. However, one fundamental characteristics of the Lorenz energy cycle – the temporal variations of the Lorenz energy cycle is not addressed in the previous investigations including the recent two studies from our research group. Therefore, we will investigate the temporal variations of the Lorenz energy cycle in this study. The two datasets (NCEP and ECWMF) used in our two studies (Li, Ingersoll et al. 2007, Li, Jiang et al. 2011) recently experienced significant updates. In addition, the time periods covered by the updated datasets are longer than the time periods of the original datasets used in our recent studies (Li, Ingersoll et al. 2007, Li, Jiang et al. 2011). Therefore, we expect that we will get not only the temporal characteristics but also more robust results for the Lorenz energy cycle of the global atmosphere.

1.4 Overview of Dissertation

In the dissertation, the latest versions of two modern satellite-based datasets (NCEP-2 and ERA-Interim) will be used to update the mean state and temporal variations of the Lorenz energy cycle of the global atmosphere during the past 35 years (1979-2013).

In the following chapters, we first introduced the theoretical framework of the Lorenz energy cycle, which will be used in our computation and analyses. The corresponding datasets and statistical tools are also introduced. Then the mean state of the Lorenz energy cycle during the past 35 years is first computed and analyzed. The updated mean state of the Lorenz energy cycle are further compared with the mean-state during the time period of 1979-2001 based on the old version of the two datasets. In the following chapter, the temporal variations of the Lorenz energy cycle are analyzed for the first time. In the last chapter, the conclusions and discussions are provided.

2 Theoretical Framework

The theory of Lorenz energy cycle and the formulation of atmospheric energies are developed in previous studies (Lorenz 1955, Oort 1964, Peixoto and Oort 1974, Li, Ingersoll et al. 2007, Li, Jiang et al. 2011). We will use the formulation and computation methods in Li, Ingersoll et al. (2007) in this research. In this chapter, we will introduce the theory and formulation of Lorenz energy cycle, the datasets (NCEP-2 and ERA-Interim) and basic idea of the computation methods. The formulas and symbols we used in this dissertation agrees with Peixoto and Oort (1974), which are generalized from the theoretical concepts (Lorenz 1955) in the mixed space-time domain (Oort 1964). The four energy components (P_M, P_E, K_M, and K_E), and four conversions ($C(P_M, P_E)$, $C(P_E, K_E)$, $C(K_E, K_M)$, and $C(P_M, K_M)$) are directly calculated from the formulation. The two generation terms ($G(P_M)$, and $G(P_E)$), and two dissipation terms ($D(K_M)$, and $D(K_E)$) are calculated by assuming the balanced Lorenz energy cycle.

2.1 Analytic Expressions of Available Potential Energy and Kinetic Energy

Lorenz first introduced Lorenz energy cycle with analytic analysis in 1950s. The key point for Lorenz energy cycle is the definition and analytic expression of available potential energy. Available potential energy is part of potential energy that could convert into kinetic energy, which equals the maximum gain of kinetic energy under any adiabatic redistribution of mass. Based on the definition, Lorenz summarized four important properties of available potential energy (Lorenz 1955):

(1) The sum of the available potential energy and kinetic energy is conserved under adiabatic flow. This is the law of conservation of (mechanical) energy in the atmospheric energy system.

(2) The available potential energy is completely determined by the distribution of mass. This means the available potential energy is a function of position and the distribution of mass is the only variable of the available potential energy. In the calculation of this research, we will use a relationship between mass distribution and temperature to redefine the expression of available potential energy as a function of temperature.

(3) The available potential energy is zero if the mass distribution is horizontal and statically stable. This is the definition of zero available potential energy, which is the lowest it can reach with adiabatic redistribution of mass.

(4) The available potential energy is positive if the stratification is not both horizontal and statically stable. This means the available potential energy could be only positive if any mass distribution is unstable. The (3) and (4) together tell us that the available potential energy could be only non-negative.

By this definition of available potential energy, it doesn't mean the total available potential energy could convert into kinetic energy for any individual case. This is applied for the ideal case, which deviates from the real case. But this is still very meaningful in physics and convenient for calculation. By this definition, available potential energy and kinetic energy could be divided into two parts, which are function of position (temperature) and function of velocities separately.

With the definition, we have the analytic expression of available potential energy over a unit area as

$$Available\ Potential\ Energy = \frac{1}{2}\int \bar{T}(\Gamma_d - \bar{\Gamma})^{-1}\overline{\left(\frac{T'}{\bar{T}}\right)^2}\, dp \qquad (2-1)$$

or

$$Available\ Potential\ Energy = \frac{1}{2}c_p \int \gamma[\bar{T}''^2]\, dm$$

where $\bar{T}$ is the average of temperature, T' is temperature departure from average of temperature, Γ_d is dry-adiabatic lapse rate and $\bar{\Gamma}$ is lapse rate and dp is the integral element of pressure.

And the analytic expression of kinetic energy over a unit area is defined as

$$Kinetic\ Energy = \frac{1}{2} g^{-1} \int \overline{V^2}\, dp \qquad (2-2)$$

or

$$Kinetic\ Energy = \frac{1}{2} \int \overline{V^2}\, dm$$

where g is the gravitational acceleration, V is velocity, dp is the integral element of pressure and dm is the integral element of mass.

In this definition, we could estimate the ratio between kinetic energy and available potential energy:

$$\frac{Kinetic\ Energy}{Available\ Potential\ Energy} \sim {}^{1}/_{10}$$

2.2 Expressions in Space, Time and Mixed Domain

In equations (2-1), and (2-2), we already defined the expression of available potential energy and kinetic energy. To further study about the details about atmospheric energies, we expand the expression in space, time or mixed domain (Oort 1964).

First, the eastward and northward components of the wind (velocity) u, and v, and the temperature T can be written as the sum of four components:

$$u = [\bar{u}] + \bar{u}^* + [u]' + u'^*$$

$$v = [\bar{v}] + \bar{v}^* + [v]' + v'^*$$

$$T = [\bar{T}] + \bar{T}^* + [T]' + T'^*$$

Where the brackets represent a zonal average, the star is a deviation from the zonal average, the bar is a time average and the prime is a deviation from the time average. We could use 0, 1, 2, and 3 to label four parts of energies corresponding to the four components of velocities and temperature. Then we can separate kinetic energy and available potential energy into mean and eddy parts in three different methods (space, time and mixed domain):

(1) Space domain:

$$K_{M(space)} = K_0 + K_2 = \frac{1}{2}\int \overline{([u]^2 + [v]^2)}\, dm$$

$$K_{E(space)} = K_1 + K_3 = \frac{1}{2}\int \overline{([u^{*2}] + [v^{*2}])}\, dm$$

$$P_{M(space)} = P_0 + P_2 = \frac{1}{2}c_p \int \overline{\gamma [T]''^2}\, dm$$

$$P_{E(space)} = P_1 + P_3 = \frac{1}{2}c_p \int \overline{\gamma [T^{*2}]}\, dm$$

These four components in space domain are also defined in (Lorenz 1955) as zonal and eddy kinetic / available potential energy.

(2) Time domain:

$$K_{M(time)} = K_0 + K_1 = \frac{1}{2}\int [\bar{u}^2 + \bar{v}^2]\, dm$$

$$K_{E(time)} = K_2 + K_3 = \frac{1}{2}\int \left[\overline{u'^2} + \overline{v'^2}\right] dm$$

$$P_{M(time)} = P_0 + P_1 = \frac{1}{2}c_p \int \gamma [\bar{T}''^2]\, dm$$

$$P_{E(time)} = P_2 + P_3 = \frac{1}{2}c_p \int \gamma \left[\overline{T'^2}\right] dm$$

(3) Mixed space-time domain:

$$K_M = K_0 = \frac{1}{2}\int ([\bar{u}]^2 + [\bar{v}]^2)\, dm$$

$$K_E = K_1 + K_2 + K_3 = \frac{1}{2}\int \left[\overline{u'^2} + \overline{v'^2} + \bar{u}^{*2} + \bar{v}^{*2}\right] dm$$

$$P_M = P_0 = \frac{1}{2} c_p \int \gamma [\bar{T}]''^2\, dm$$

$$P_E = P_1 + P_2 + P_3 = \frac{1}{2} c_p \int \gamma \left[\overline{T'^2} + \bar{T}^{*2}\right] dm$$

where

$$c_p = \text{specific heat at constant pressure}$$

$$\gamma = -(\theta/T)\left(R/c_p p\right)\left(\partial\left[\langle\tilde{\theta}\rangle\right]/\partial p\right)^{-1} = \Gamma_d [\langle\tilde{T}\rangle]^{-1}\left(\Gamma_d - \left[\langle\tilde{\Gamma}\rangle\right]\right)^{-1}$$

The third method (mixed space-time domain) is used in the calculation. The definitions of mean and eddy energies are introduced in Chapter 1. By definition, eddy energy considers eddies in both space and time domains. Mean energy is averaged over both time and space domains. The average in time could be monthly average or yearly average, which depends on the data and studies. In our research, we use monthly mean data, so the mean energies represent average of monthly data in time domain and zonal average (average in latitude circles) in spatial domain. Available potential energy, and kinetic energy are separated into two parts: mean, and eddy energies. Mean energies are

describing large-scale processes in space and long-term in time and eddy energies refer to small-scale processes in space and short-term in time.

2.3 Formulation of Lorenz Energy Cycle

The definition has been showed in Section 2.2 and in this section we will introduce the formulation of Lorenz energy cycle. In this dissertation, we use the same notation and formulation as Peixoto and Oort (1974). To discuss the basic quantities in Lorenz energy cycle, we will use the formulation for four energy components and four conversion rates. The generations and dissipations are calculated by assumption of balanced Lorenz energy cycle. Boundary conditions (Peixoto and Oort 1974) will not be used since this study is using the datasets with global coverage (no equator boundary condition needed).

The following notation will be used:

a	average radius of the earth;
c_p	specific heat at constant pressure;
$C(P, K)$	conversion rate of P into K;
dm	mass element, equal to $\frac{a^2 cos\phi}{g} d\lambda\, d\phi\, dp$;
dx	$a\, cos\phi\, d\lambda$
dy	a dφ
$D(K)$	dissipation rate of K;
f	Coriolis parameter, equal to $2\Omega\, sin\phi$;
g	acceleration resulting from gravity;
$G(P)$	generation rate of P;
K	kinetic energy;
K_M, K_E	mean, eddy kinetic energy;
$K_{TE,} K_{SE}$	transient, stationary eddy kinetic energy;
p	pressure;
P	available potential energy;
P_M, P_E	mean, eddy available potential energy;
P_{TE}, P_{SE}	transient, stationary eddy available potential energy;
Q	adiabatic heating rate (latent heating plus radiational cooling plus boundary layer heating);
R	gas constant (for dry air);

t time;

T temperature;

u zonal wind component (positive if it is eastward);

u_g geostrophic zonal wind component, equal to $-gf^{-1}(\partial Z/a\partial\phi)$;

v meridional wind component (positive if it is northward);

$\boldsymbol{v}$ horizontal vector wind , equal to $ui + vj$;

ω vertical velocity

Z 'geopotential' height;

γ stability factor, equal to $-\left(\frac{\theta}{T}\right)\left(\frac{R}{c_{pp}}\right)\left(\frac{\partial[\langle\tilde{\theta}\rangle]}{\partial p}\right)^{-1} = \Gamma_d[\langle\tilde{T}\rangle]^{-1}\left(\Gamma_d - [\langle\tilde{\Gamma}\rangle]\right)^{-1}$;

Γ lapse rate, equal to $-\partial T/\partial z$;

κ R/c_p;

λ geographic longitude;

ϕ geographic latitude;

$\langle A\rangle$ time average of A, equal to $\frac{1}{t_2-t_1}\int_{t_1}^{t_2} A\,dt$;

A' departure from time average of A, equal to $A - \langle A\rangle$;

$[A]$ zonal average of A, equal to $\frac{1}{2\pi}\int_0^{2\pi} A\,d\lambda$;

A^* departure from zonal average of A, equal to $A - [A]$;

$\widetilde{A}$ meridional average of A, equal to $\int_{-\frac{\pi}{2}}^{\frac{\pi}{2}} A\cos\phi\,d\phi$;

A'' deviation from meridional average of A equal to $A - \widetilde{A}$.

The formulation of energy components and conversion rates are:

Mean available potential energy:

$$P_M = \frac{c_p}{2} \int \gamma \left(\left[\langle T \rangle \right]'' \right)^2 dm$$

Eddy available potential energy:

$$P_E = \frac{c_p}{2} \int \gamma \left\{ \left\langle \left(T' \right)^2 \right\rangle + \left(\langle T \rangle^* \right)^2 \right\} dm$$

$$P_E = P_{TE} + P_{SE}$$

Mean kinetic energy:

$$K_M = \frac{1}{2} \int \left\{ \left[\langle u \rangle \right]^2 + \left[\langle v \rangle \right]^2 \right\} dm$$

Eddy kinetic energy:

$$K_E = \frac{1}{2} \int \left\{ \left\langle \left(u' \right)^2 \right\rangle + \left\langle \left(v' \right)^2 \right\rangle + \left(\langle u \rangle^* \right)^2 + \left(\langle v \rangle^* \right)^2 \right\} dm$$

$$K_E = K_{TE} + K_{SE}$$

Conversion rates:

$$C(P_M, P_E) = -c_p \int \gamma[\langle v'T' \rangle + \langle v \rangle^* \langle T \rangle^*] \frac{\partial[\langle T \rangle]}{a\,\partial\phi} dm$$

$$-c_p \int p^{-\kappa}[\langle \omega'T' \rangle + \langle \omega \rangle^* \langle T \rangle^*] \frac{\partial(\gamma p^{\kappa}[\langle T \rangle]'')}{\partial p} dm$$

$$C(P_E, K_E) = -\int g \left(\left[\langle \frac{u'\partial Z'}{a\,cos\phi\,\partial\lambda} \rangle + \langle \frac{v'\partial Z'}{a\,\partial\phi} \rangle \right] + \left[\frac{\langle u \rangle^* \partial \langle Z \rangle^*}{a\,cos\phi\,\partial\lambda} + \frac{\langle v \rangle^* \partial \langle Z \rangle^*}{a\,\partial\phi} \right] \right) dm$$

$$C(K_E, K_M) = \int [\langle v'u' \rangle + \langle v \rangle^* \langle u \rangle^*]\, cos\phi \left\{ \frac{\partial([\langle u \rangle]/cos\phi)}{a\,\partial\phi} \right\} dm$$

$$+ \int \left[\langle v'^2 \rangle + \langle v \rangle^{*2} \right] \frac{\partial[\langle v \rangle]}{a\,\partial\phi} dm + \int [\langle \omega'u' \rangle + \langle \omega \rangle^* \langle u \rangle^*] \frac{\partial[\langle u \rangle]}{\partial p} dm$$

$$+ \int [\langle \omega'v' \rangle + \langle \omega \rangle^* \langle v \rangle^*] \frac{\partial[\langle v \rangle]}{\partial p} dm - \int [\langle v \rangle] \left(\left[\langle u'^2 \rangle + \langle u \rangle^{*2} \right] \right) \frac{tan\phi}{a} dm$$

$$C(P_M, K_M) = -\int [\langle v \rangle]\, g \frac{\partial[\langle Z \rangle]}{a\,\partial\phi} dm$$

And for generations and dissipations, we have the formulation with balancing of energy flows:

Generation of mean available potential energy:

$$G(P_M) = C(P_M, P_E) + C(P_M, K_M)$$

Generation of eddy available potential energy:

$$G(P_E) = -C(P_M, P_E) + C(P_E, K_E)$$

Dissipation of mean kinetic energy:

$$D(K_M) = C(P_M, K_M) + C(K_E, K_M)$$

Dissipation of eddy kinetic energy:

$$D(K_E) = C(P_E, K_E) - C(K_E, K_M)$$

2.4 Datasets and Methods of Computation

2.4.1 Datasets

The datasets we used in this study are NCEP-DOE Reanalysis 2 (NCEP-2) from the National Centers for Environmental Prediction — National Center for Atmospheric Research (NCEP-NCAR) (Kalnay, Kanamitsu et al. 1996, Kanamitsu, Ebisuzaki et al. 2002) and ERA-Interim from the European Center for Medium-Range Weather Forecasts (ECMWF) (Uppala 2002, Uppala, Kallberg et al. 2005, Dee, Uppala et al. 2011).

In this study, we use geopotential height (Z), temperature (T), zonal wind component (u), meridional wind component (v), and vertical velocity (ω). Both these two datasets (NCEP-2 and ERA-Interim) have a temporal coverage of 4-times daily for January 1979 to December 2013, spatial coverage of global grids at 2.5º×2.5º latitude-longitude resolutions, and 17 pressure levels (mbar): 1000, 925, 850, 700, 600, 500, 400, 300, 250, 200, 150, 100, 70, 50, 30, 20, 10. ERA-Interim dataset are available at pressure levels up to 1 mbar. In this research we only use the data below 10 mbar level to match with NCEP-2 dataset.

The wind components (u, and v), and vertical velocity (ω) data are used in the computation of kinetic energies. Temperature data is used in computation of available potential energies. Both velocity, and temperature data are used in the computation of conversion rates.

2.4.2 Methods of Computation

The basic method of computation is based on the analysis of expressions and formulations discussed in Sections 2.2, and 2.3. A numerical integration method is used in the computation using MatLab scripts. All calculations are based on the 3D spatial grids (pressure level, latitude, and longitude) of NCEP-2 dataset. A linear interpolation is applied on ERA-Interim data in pressure levels (no interpolation is needed in latitude or longitude where NCEP-2, and ERA-Interim datasets have same coverage and resolutions).

To investigate mean states of Lorenz energy cycle, we first calculate the temporal average of energy components, and conversion rates over 2D (pressure level, and latitude) or 3D (pressure level, latitude, and longitude) space domain using equations discussed in Section 3.3. Then we calculate the global mean (Figure 3.1) to study the global mean states of Lorenz energy cycle and take weighted zonal average or integration on pressure

levels to explore the spatial structures of energy components (Figures 3.2, 3.3, 3.4, and 3.5) and conversion rates (Figures 3.6, 3.7, 3.8, and 3.9).

To explore the temporal variations (trends, and time series) of Lorenz energy cycle, we compute energy components and conversion rates at each spatial grid for each month. Each energy component and conversion rate has a time series on each spatial grid. After removing the seasonal cycle, high frequency signals, and El Nino-Southern Oscillation signal in each time series, we calculate the trends for each time series at each spatial grid. Same methods are used in the analysis of spatial structures of trends. For time series analysis, we plot the original time series of each energy component and each conversion rate with the global mean (only in space) of energy components and conversion rates data in each month. Then we remove the seasonal cycle, smooth the data with low-pass filter, apply the multiple regression, and compare data in different time periods.

3 Mean States of Lorenz Energy Cycle

The Lorenz energy cycle is a cycle of energy flows/conversions in the atmosphere, which plays a key role in the atmospheric system and, at a large-scale level, has a very big influence on climate and weather changes. The research for the investigation of mean states of Lorenz energy cycle is very important. Many researches (Krueger, Winston et al. 1965, Wiinniel.A, Steinber.L et al. 1967, Oort and Peixoto 1974, Peixoto and Oort 1974, Oort and Peixoto 1976, Oort 1983, Sheng and Hayashi 1990, Hu, Tawaye et al. 2004) estimated the mean states of Lorenz energy cycle based on limited surface observation. These investigators reported a brief approximation of the Lorenz energy cycle. Further analysis for details of the Lorenz energy cycle is needed with reliable observations with high resolution, precision, and with global coverage.

Two reanalysis datasets from the National Centers for Environmental Prediction - National Center for Atmospheric Research (NCEP-NCAR) and the European Center for Medium-Range Weather Forecasts (ECMWF) were produced with global coverage since the 1950s (Kalnay, Kanamitsu et al. 1996, Kanamitsu, Ebisuzaki et al. 2002, Uppala 2002, Uppala, Kallberg et al. 2005, Dee, Uppala et al. 2011). These records were derived

from different data sources. High precision and reliable satellite datasets were available since 1979. A recent study in our group evaluated mean states of the Lorenz energy cycle with data from 1979 to 2001 (Li, Ingersoll et al. 2007). This research showed a consistent result as compared to some previous results(Oort and Peixoto 1974, Peixoto and Oort 1974, Oort 1983, Sheng and Hayashi 1990, Peixoto and Oort 1992, Hu, Tawaye et al. 2004). In addition, it revealed a new discovery: a positive value for the conversion from P_M to K_M ($C(P_M, K_M)$).

In this chapter, I will use two newest datasets (NCEP-2, and ERA-Interim) to examine the mean states of Lorenz energy cycle and calculate the spatial distributions of the Lorenz energy cycle. I will use both datasets from 1979 to 2013. The temporal coverage is about 1.5 times to the previous research (Li, Ingersoll et al. 2007). Results shown in this chapter can help understand if the Lorenz energy cycle changes in recent years.

3.1 Mean States of the Lorenz Energy Cycle

This section analyzes the four energy components (P_M, P_E, K_M, and K_E) and four conversion rates ($C(P_M, P_E)$, $C(P_E, K_E)$, $C(K_E, K_M)$, and $C(P_M, K_M)$) in the Lorenz energy cycle for each cross-section in the spatial domain using monthly data from January 1979 to December 2013. A weighted (for different latitudes) average for both spatial and temporal domains are evaluated. The values of these four energy components (P_M, P_E, K_M, and K_E) and their conversion rates ($C(P_M, P_E)$, $C(P_E, K_E)$, $C(K_E, K_M)$, and $C(P_M, K_M)$) are calculated directly using formulas discussed in Sections 2.2 and 2.3. The values of generations of available potential energies and dissipations of kinetic energies (in parentheses) are estimated by balancing Lorenz energy cycle. Figure 3.1 illustrates the mean state results from two datasets averages (NCEP-2, and ERA-Interim) from two different data periods (1979-2013 and 1979-2001).

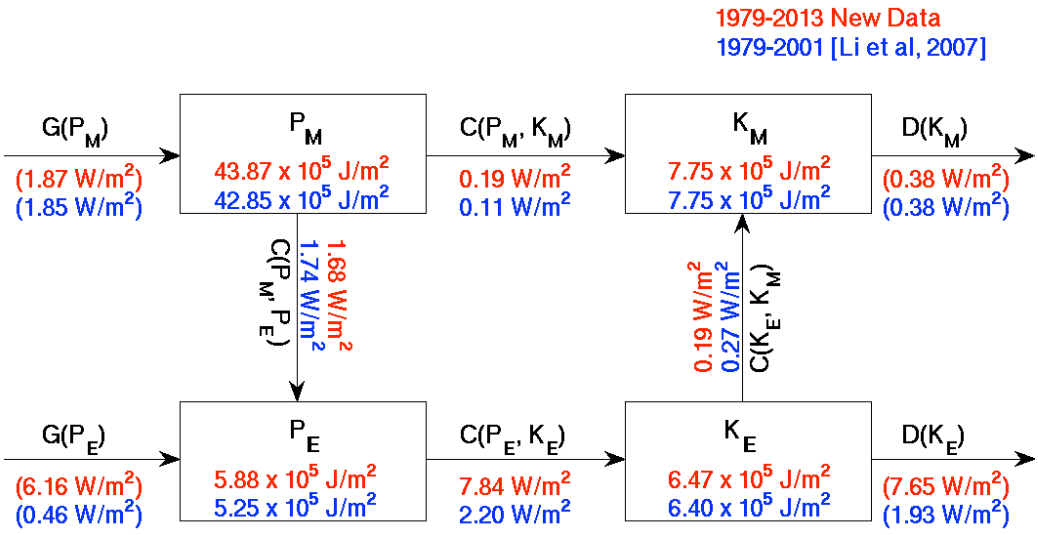

Figure 3.1 Lorenz energy cycle in two different time periods (1979-2013 and 1979-2001). Numbers in red and blue are the new results from this research and the old results from our previous study (Li et al., 2007), respectively. The values shown in this figure are the global-average time-mean results. In addition, the results are averaged over the two data sets (i.e., NCEP-2 and ERA-Interim). The energy components (P_M, P_E, K_M, and K_E) and conversion rates ($C(P_M, P_E)$, $C(P_E, K_E)$, $C(K_E, K_M)$, and $C(P_M, K_M)$) are calculated directly from the equations in Chapter 2. The generations ($G(P_M)$, and $G(P_E)$) and dissipations ($D(K_M)$, and $D(K_E)$) in parentheses are estimated by balancing the Lorenz energy cycle.

Both red and blue values are averages of two datasets (NCEP-2, and ERA-Interim). The red values are the new results from the new data over 1979-2013, and the blue values are the results from Li, Ingersoll et al. (2007). These two results are consistent in most atmospheric energies and conversions. The only noticeable difference is in

$C(P_E, K_E)$, which may be due to different time coverage, and some discrepancy in the different data versions (both NCEP and ERA datasets released new versions since 2007).

P_M is 43.87×10^5 J/m^2, and 42.85×10^5 J/m^2 from the new data results and previous results, respectively. The difference between these two results is about 2%. P_M is the dominant term in the whole atmospheric mechanical energy, which accounts for more than two thirds of the global atmospheric mechanical energy. Its mean state value is about 6 to 8 times more as compared to other energy components. K_M is 7.75×10^5 J/m^2 in both results. The results are almost the same in these two calculations over 1979-2013 and 1979-2001. K_M mainly comes from atmosphere motions due to P_M and also some exchanges with K_E. P_E is 5.88×10^5 J/m^2, and 5.25×10^5 J/m^2 from the new data results and previous results, respectively. The sources of P_E are from the differences of the solar radiation heating in different atmospheric areas and transferring from P_M. K_E is 6.47×10^5 J/m^2, and 6.40×10^5 J/m^2 from the new data results and previous results, respectively. The difference between them is about 1%. The main sources of K_E are air motions related with energy release from P_E and energy exchanges with K_M. All energy components are showing almost the same mean states in these two results, which suggests that the new result is reliable and the Lorenz energy cycle retains these main features in mean states. The conversion rate $C(P_M, P_E)$ is 1.68 W/m^2, and 1.74 W/m^2 from the new data results and previous results, respectively; conversion rate $C(P_E, K_E)$ is 7.84 W/m^2, and 2.20 W/m^2 from the new data results and previous results, respectively; conversion rate $C(K_E, K_M)$ is 0.19 W/m^2, and 0.27 W/m^2 from the new data results and previous results, respectively; and conversion rate $C(P_M, K_M)$ is 0.19 W/m^2, and 0.11 W/m^2 from the new

data results and previous results, respectively. Most of the conversions also have similar mean values except the conversion between P_E and K_E. This indicates that these two datasets (different time periods, and different versions) maintain most features, and may update the precisions in some variables such as air temperature, and wind velocities. One possible reason of the difference in $C(P_E, K_E)$ may be that the new datasets have new vertical velocities, or higher precision at small scales. The generations and dissipations in parentheses are calculated by balancing the connected conversions. The energy sources in the Lorenz energy cycle are generations of available potential energies, and the energy sinks departing from the Lorenz energy cycle are dissipations of kinetic energies related to the frictional forces.

The generations, dissipations, and conversions keep energy flows in the Lorenz energy cycle. The relative constant temperature distributions and atmospheric motions are contributing to the mean states of energy components.

3.2 Spatial Distributions of the Four Energy Components

The Lorenz energy cycle is a global scale energy cycle, which has its 3D structure (pressure level, latitude, and longitude). Available potential energies could vary in different locations because the solar radiation differ in latitudes, and, also, land and sea have different heat capacities, which would lead to a temperature distribution in 3D

structure. The 3D temperature structure determines the available potential energies in different resions. Kinetic energies would also have a unique structure related to the distribution of available potential energies, and surface conditions, which would contribute to the wind velocities.

Of the four energy components, both P_M and K_M already include an average in latitude circles (averages of different longitudes with same latitude). These two components are 2D structures (pressure level, and latitude), which mainly stand for large scales both in space and time of available potential energy and kinetic energy. In addition, the two eddy energies (P_E, and K_E) are 3D structures, which stand for small scales both in space and time.

3.2.1 2D Structure of P_M

P_M is the dominant term in the Lorenz energy cycle. It mainly originates from solar radiation (absorbed directly from sun or via surface). The structure of P_M is determined by the distribution of solar radiation absorption in latitudes and pressure levels.

Figure 3.2 is a 2D structure (pressure level and latitude) of the 35-year mean state of P_M. P_M is primarily in regions with large temperature departures to the global mean temperature (polar regions and equator). The highest level of P_M is located in the two

Polar Regions near the surface and especially the South Pole. These areas have the largest temperature departures to the global mean temperature. The 2D structure shows that P_M in the South Pole region is much stronger than the North Pole, because the South Pole is much colder than the North Pole. P_M has a higher value near the surface region than higher levels since the temperature difference near surface is larger than upper levels. P_M over most of other regions is much weaker than the polar surface regions.

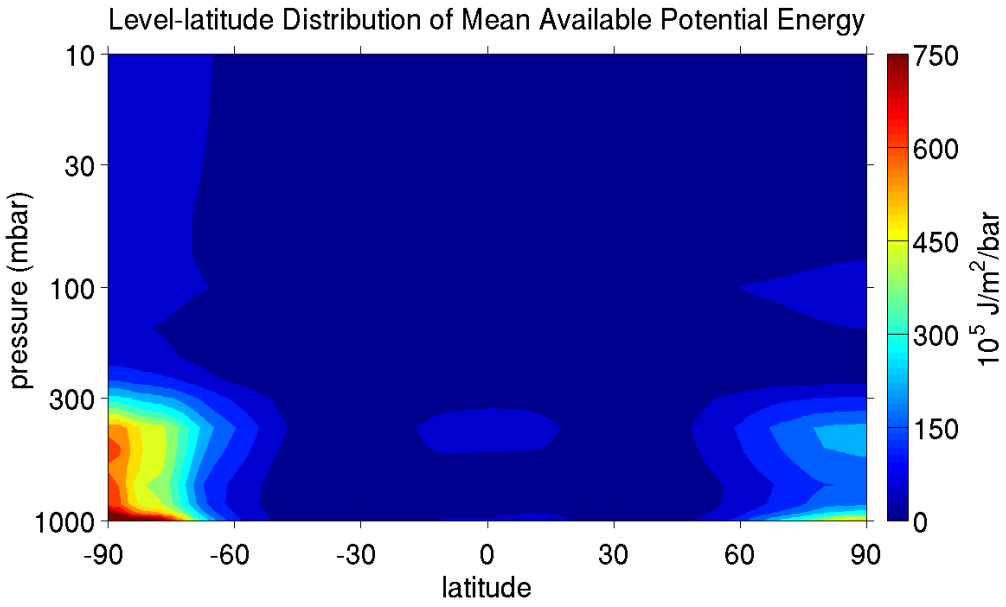

Figure 3.2 Pressure-latitude cross section of mean available potential energy (P_M). This figure is an average of the monthly evaluation of the two data sets (i.e., NCEP-2, and ERA-Interim) during the past 35 years (1979-2013).

3.2.2 2D Structure of K_M

K_M is the large-scale representation of kinetic energy, which describes the atmospheric motions at a large or global scale. The characterization of K_M is large-scale air motions, which are related to the energy converted from P_M, and other air motions (e.g. K_E, Coriolis Effect).

Figure 3.3 depicts a 2D structure of the 35-year mean state of K_M. The highest values of K_M are located at the mid-latitudes in both troposphere and stratosphere, and in both the Northern Hemisphere (NH) and the Southern Hemisphere (SH). The high values of K_M are in the areas with strong atmospheric circulations. The centers of K_M are at the same locations where the tropospheric jet streams and stratospheric jet streams are located. In the stratosphere, the center in the SH is much stronger than in the NH is because the center in the NH is higher than the pressure level of 10 mbar (the highest level of data in this research). Furthermore, the center of K_M in the troposphere of the SH is also stronger than in the NH. The physics behind this phenomenon could be that the less land-ocean difference in the SH makes the air motions much smoother than in the NH, which has a more complex land-ocean difference or high mountains on the surface. And we could see the opposite phenomenon in K_E, which has a higher value in the NH than in the SH.

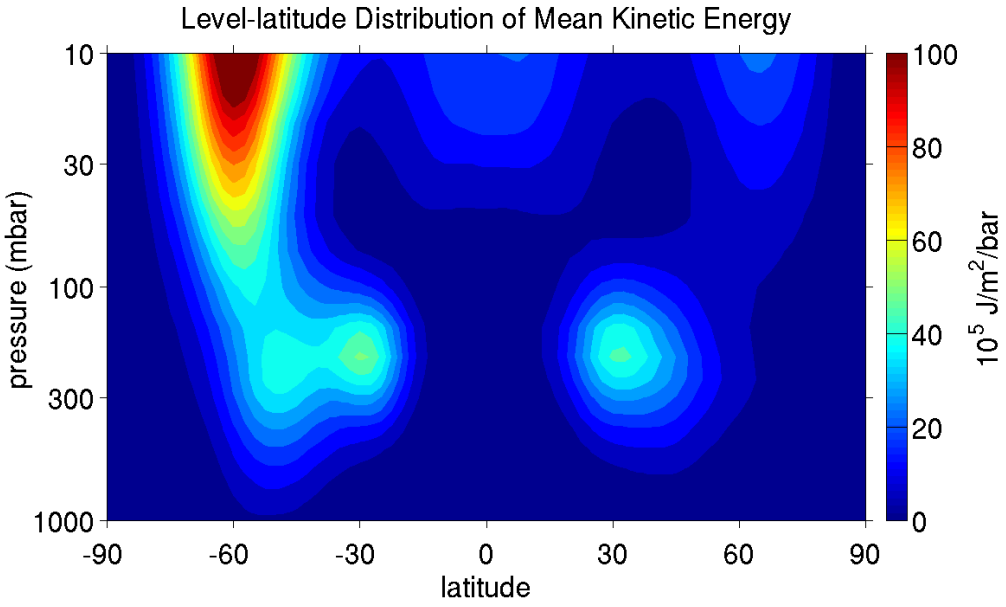

Figure 3.3 Same as Fig. 3.2 except for the mean kinetic energy (K_M).

3.2.3 3D Structure of P_E

In contrast to the mean energies with 2D structures, there is a 3D structure (pressure level, latitude, and longitude) for P_E. The 3D structure of P_E shows some details in the small scales of available potential energy.

Figure 3.4 (a) shows the pressure level-latitude structure of the 35-year mean state of P_E. The maxima of P_E are near the maxima of P_M with a slight displacement to the equator. The maxima of P_E are located in the mid-latitudes near the surface, which are in the regions of strong temperature perturbation in the zonal direction (latitude circle).

Further details of level-latitude distribution of P_E are shown in Figure 3.4 (b) with a global distribution of the 35-year mean state of P_E. As shown in Figure 3.4 (b), the maxima of P_E in the NH are over the coasts of Asia, and North America; the maxima of P_E in the SH are near the boundaries of Antarctica. These areas with maxima of P_E are the land-ocean boundaries with high temperature contrasts.

Moreover, Figure 3.4 (b) also shows high values of P_E (shown in dark red) in Tibetan Plateau, Greenland, and Andes areas. These high values of P_E could be related to the original data in ERA-Interim dataset, or the high altitudes in these areas.

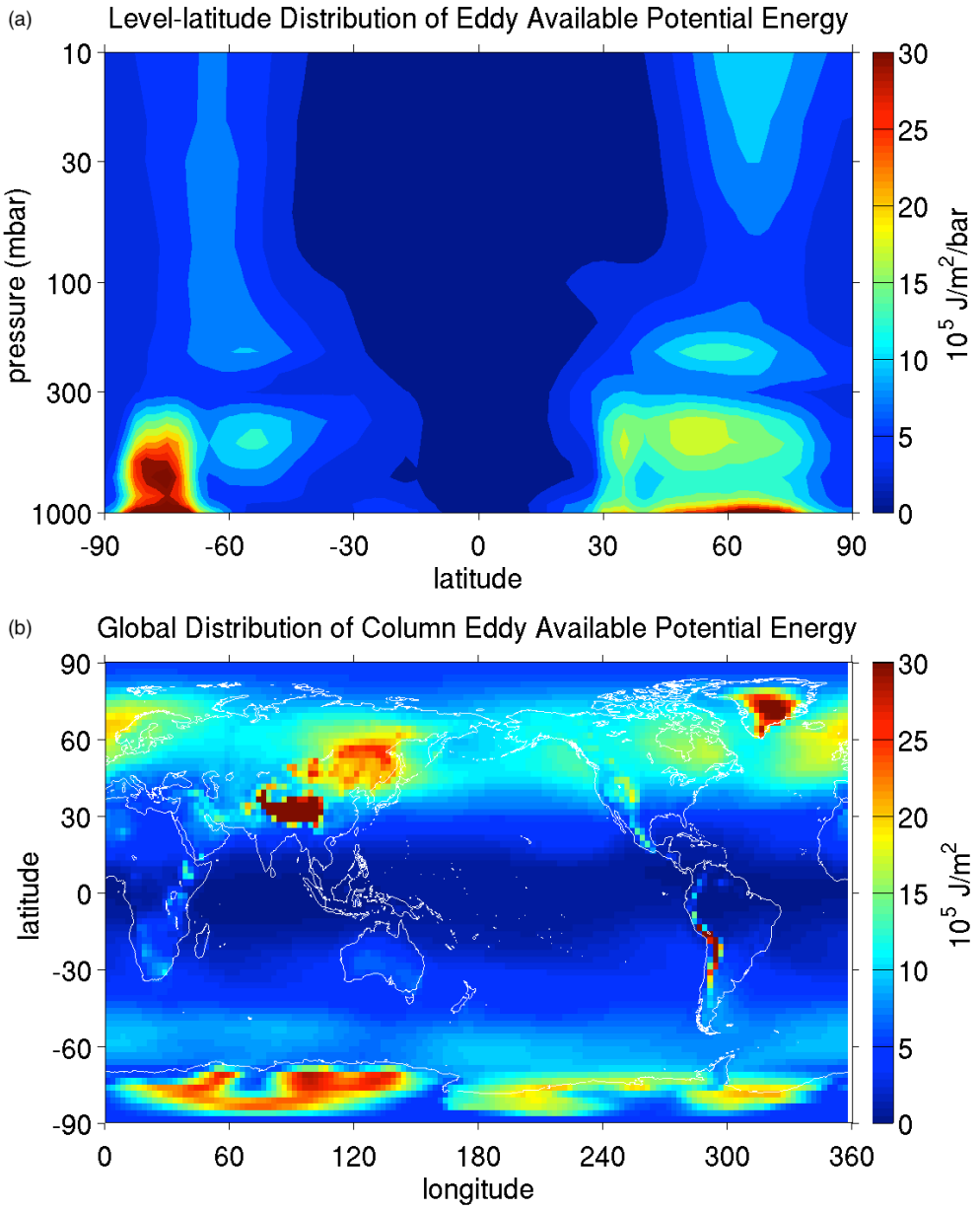

Figure 3.4 Spatial distribution of eddy available potential energy (P_E). This figure shows the time-mean (1979-2013) values. (a) pressure-latitude cross section, and (b) global distribution in latitude-longitude map. P_E is 3-dimension (pressure-latitude-longitude) structure, and the 3-D structure is averaged over one dimension to get the structure in the other 2-dimension cross section.

3.2.4 3D Structure of K_E

The mean state of K_E also has a 3D structure. Figure 3.5 (a) is a pressure level-latitude structure of the 35-year mean state of K_E. The centers of maxima for K_E are located between the centers of K_M, and P_E. The structure of K_E is affected by K_M with a slight displacement to the poles, and also affected by P_E with the synoptic cyclones controlled by the temperature perturbations. A difference between K_E and K_M is the strength showing opposite phenomenon in two hemispheres. The centers of K_E in the NH are stronger than the SH, which is also due to the complexity of the surface condition. The storms and eddies in the troposphere, and wave in the stratosphere are much stronger in the NH and these small-scale air motions (storms, eddies, and waves) make more eddy energy in these areas.

Figure 3.5 (b) is a global distribution of the 35-year mean state of K_E. This figure shows more details about the centers of K_E. The centers of K_E in the NH are in the areas of two storm tracks over the Pacific and the Atlantic Oceans (Ulbrich, Pinto et al. 2008). Likewise, a belt maximum of K_E in the SH is related to the storm tracks over the Southern Oceans (Trenberth 1991, Hoskins and Hodges 2005). Many storms are in these areas, which are associated with K_E.

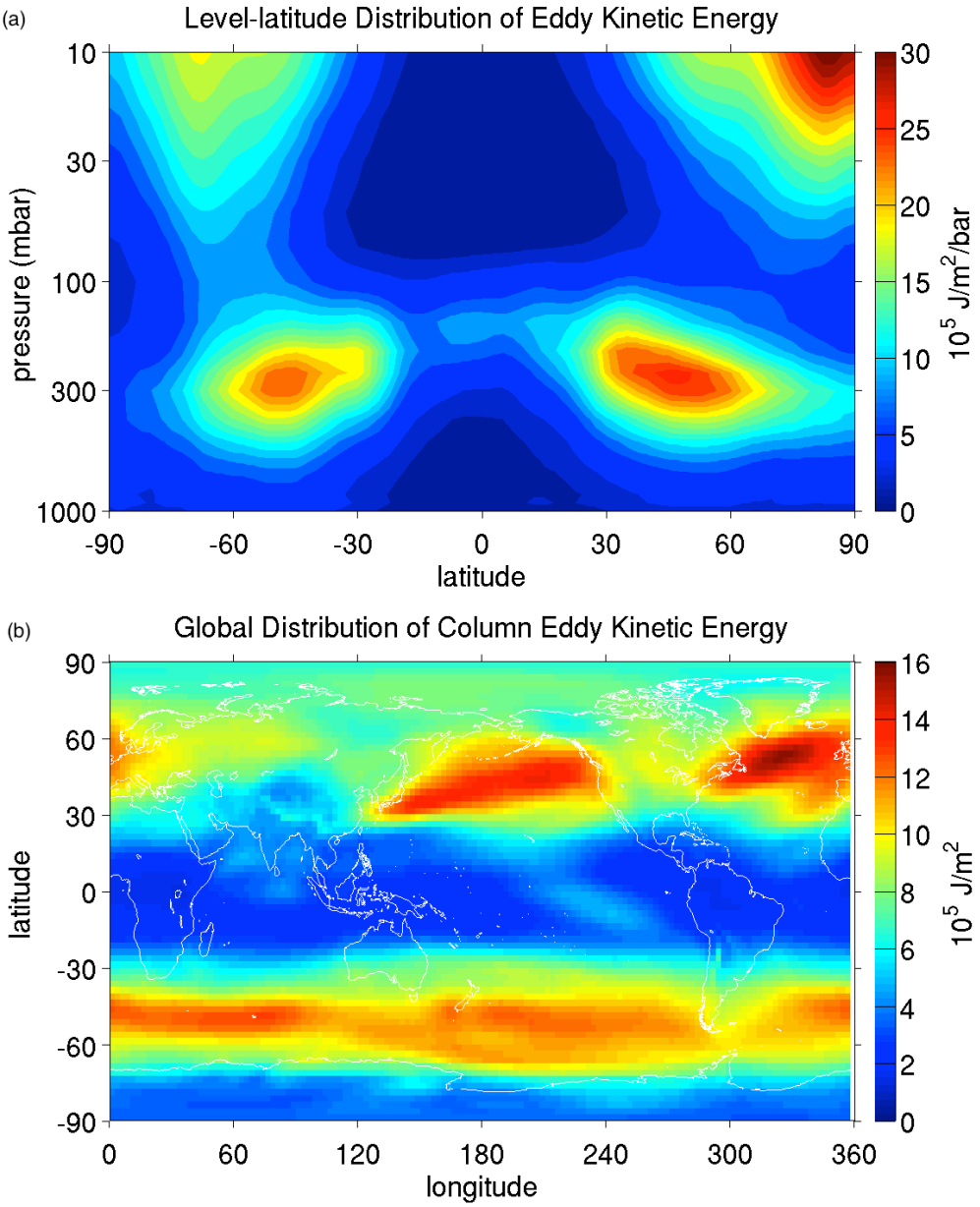

Figure 3.5 Same as Fig.3.4 except for the eddy kinetic energy (K_E).

3.3 Spatial Distributions of Four Conversions between Energy Components

The four energy components studied, K_M, P_M, K_E, and P_E, are intricately connected by the four conversions with their respective spatial structures (2D or 3D). The spatial structures of the mean states of conversions are connections to the four energy components. The energy components, conversions, generations of available potential energies, and dissipations of kinetic energies constitute the structure of the Lorenz energy cycle.

Each conversion connects two energy components. It is the relationship between these two different types of energy components that are able to interchange. The conversions could be in opposite directions (positive or negative) in different locations or at different times. The conversions are energy flows between energy components and play an important role to keep the energies in a quasi-equilibrium state.

All conversions have 2D structures (pressure level, and latitude) and the conversion ($C(P_E, K_E)$) between two eddy energies (P_E and K_E) has 3D structures (pressure level, latitude, and longitude). The structures of conversions are more complex than energy components. Because they are affected by two energy components and can be determined by both air temperature and wind velocities.

3.3.1 2D Structure of $C(P_M, P_E)$

Figure 3.6 is a 2D structure of the 35-year mean state of $C(P_M, P_E)$. The structure shows maxima of $C(P_M, P_E)$ are in the mid-latitudes of the lower troposphere in both hemispheres, which are associated with the mid-latitude cyclone activities.

This figure shows the conversion is from P_M to P_E in most locations, which means that the large-scale uniform available potential energy (temperature gradients in the meridional direction) breaks into small pieces and converts into P_E. In these locations, there are also opposite energy flows from P_E to P_M in some areas (dark blue regions).

The maximal conversion rate of $C(P_M, P_E)$ is located at the center of P_E; $C(P_M, P_E)$ is a very important source of P_E.

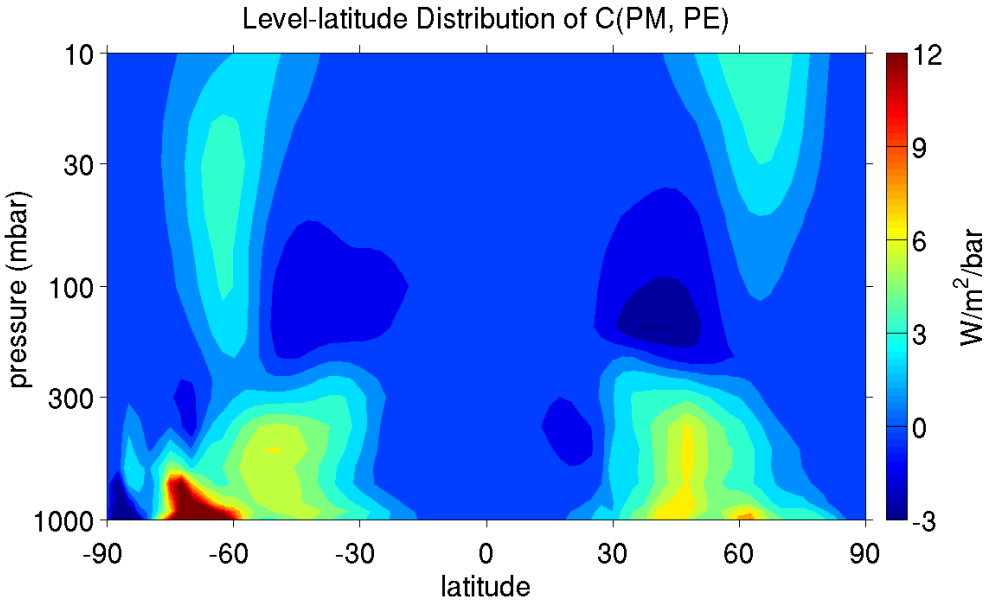

Figure 3.6 Same as Fig.3.2 except for the conversion rate $C(P_M, P_E)$.

3.3.2 3D Structure of $C(P_E, K_E)$

$C(P_E, K_E)$ is the conversion rate of P_E into K_E. This conversion is the only conversion connecting two eddy energies and has a 3D structure. $C(P_E, K_E)$ shows the conversion between potential energy and kinetic energy in small scales.

Figure 3.7 (a) is a pressure level-latitude distribution of the 35-year mean state of $C(P_E, K_E)$. There are one positive and one negative centers of $C(P_E, K_E)$ in the middle troposphere in both the NH and the SH over the mid-latitudes. This indicates that P_E converts into K_E in the lower mid-latitude and then the energy converts back into P_E in the higher mid-latitude. These are also at the same locations of centers of P_E and K_E. Likewise, the maximum of $C(P_E, K_E)$ in the South Polar region near the surface is related to the rising and sinking of air motions throughout Antarctica.

Figure 3.7 (b) is the global map of the 35-year mean state of $C(P_E, K_E)$. This figure shows that there are one positive and one negative bands of $C(P_E, K_E)$ in the mid-latitude of both hemispheres. The positive band is in the lower mid-latitude and the negative one is in the higher mid-latitude. These are the areas with the most eddy conversions, which are associated with the Ferrel cell (Ferrel cell is described on page 90 of Appendix 2).

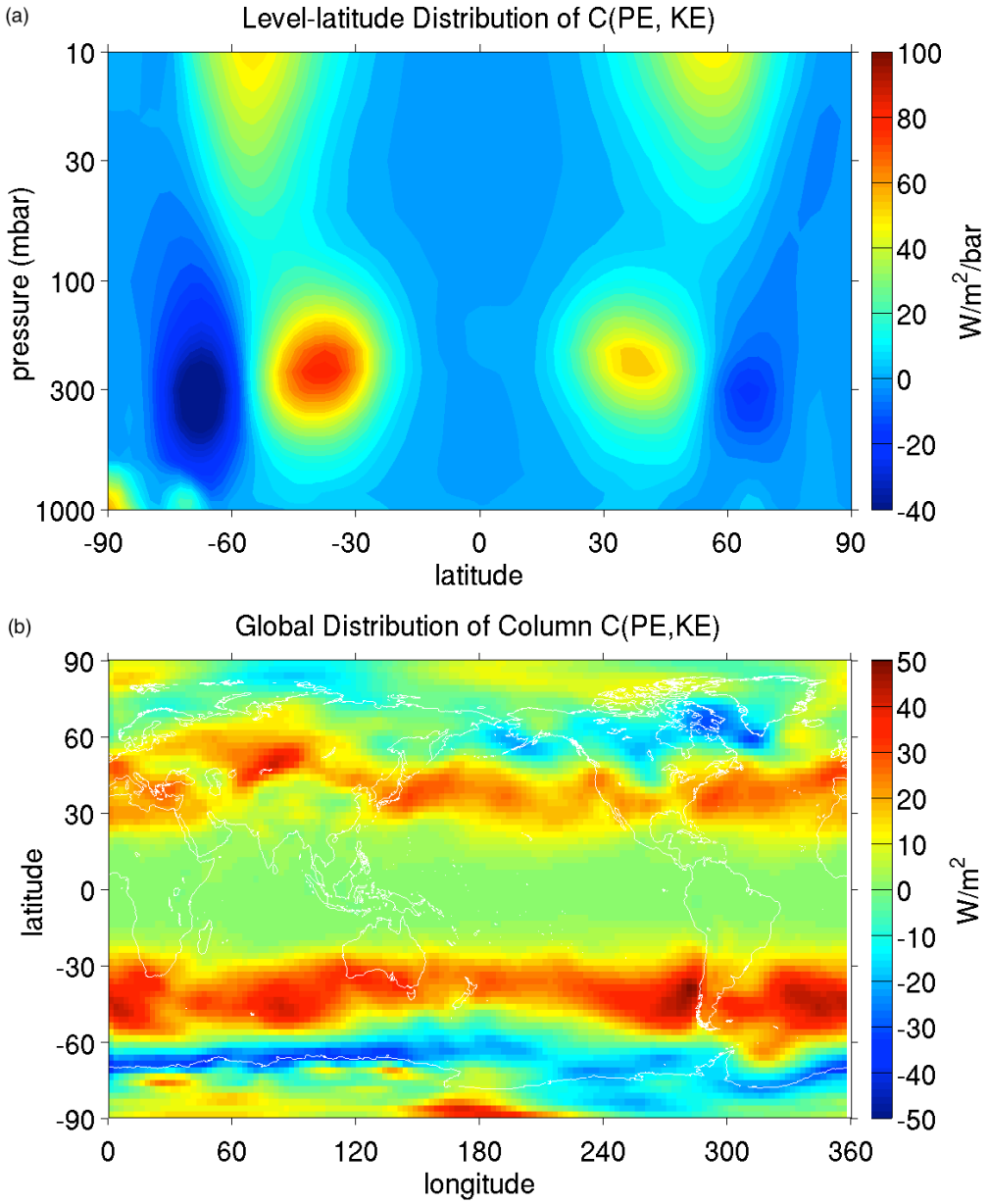

Figure 3.7 Same as Fig. 3.4 except for the conversion rate $C(P_E, K_E)$.

3.3.3 2D Structure of $C(K_E, K_M)$

Figure 3.8 is a pressure level-latitude distribution of the 35-year mean state of $C(K_E, K_M)$. The conversion rate $C(K_E, K_M)$ is the energy exchange between the kinetic energy in different scales. The centers of $C(K_E, K_M)$ are in positive-negative series in both troposphere and stratosphere. These centers are in the locations associated with atmospheric circulation and strong air motions. The centers are over all three cells (Hadley cell, Ferrel cell, and Polar cell; each are described on page 90 of Appendix 2) extending from the troposphere to the stratosphere. The kinetic energy exchanges in converting between K_M and K_E back and forth in different latitudes over the three cells are associated with the global atmospheric circulation. This figure also illustrates some local atmospheric activities related to $C(K_E, K_M)$ at the near surface, especially around the South Pole. The strong air motions in these areas lead to a strong conversion rate $C(K_E, K_M)$ between K_E and K_M.

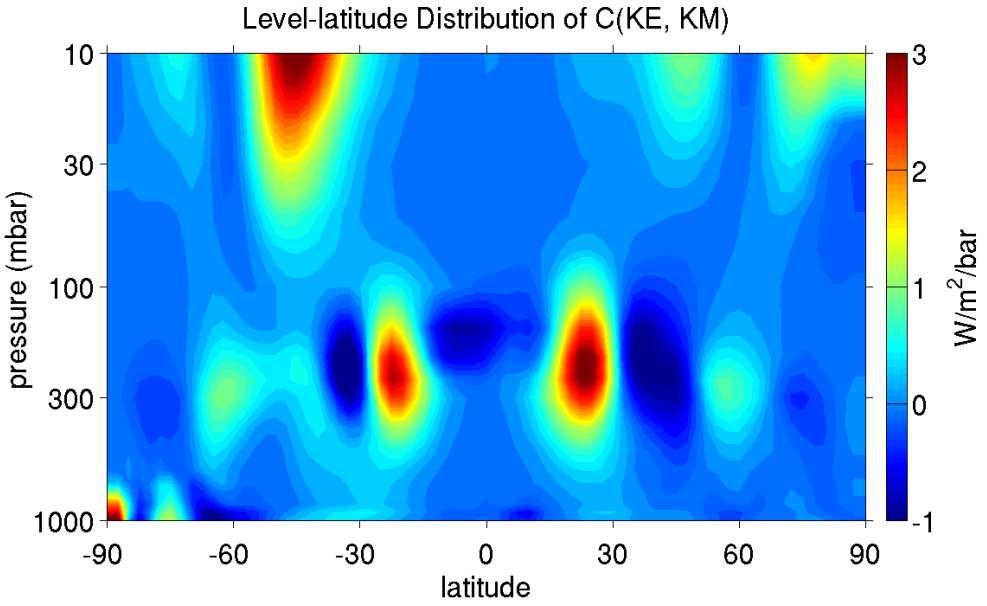

Figure 3.8 Same as Fig. 3.2 except for the conversion rate $C(K_E, K_M)$.

3.3.4 2D Structure of $C(P_M, K_M)$

The conversion rate $C(P_M, K_M)$ is the energy exchange between P_M and K_M. $C(P_M, K_M)$ connects two mean energies (large scales), which describes the global circulation between available potential energy and kinetic energy in the meridional direction.

Figure 3.9 is a pressure level-latitude distribution of the 35-year mean state of $C(P_M, K_M)$. This figure shows there are one positive and one negative centers of $C(P_M, K_M)$ in the lower mid-latitudes of the middle troposphere in both hemispheres. The positive centers are in the locations of the Hadley cell, which means air is moving from a hot area (equator) to a cold area (mid-latitude). The negative centers are in the locations of the Ferrel cell, which means air is moving from a cold area (higher mid-latitude) to a hot area (lower mid-latitude). There are also some positive centers of $C(P_M, K_M)$ in the near surface areas of the SH. These areas are centers of P_M with smooth surface conditions, which could easily convert energy into K_M.

An important discovery from Li, Ingersoll et al. (2007) is that the conversion rate $C(P_M, K_M)$ is positive for the global average, which means the energy flow direction is from P_M to K_M. It corrects The wrong direction of conversion between mean potential energy and mean kinetic energy in previous studies (e.g., (Peixoto and Oort 1974)). The

reason for the difference is that the data used in Li, Ingersoll et al. (2007) has a much better accuracy and coverage than previous studies (Peixoto and Oort 1974).

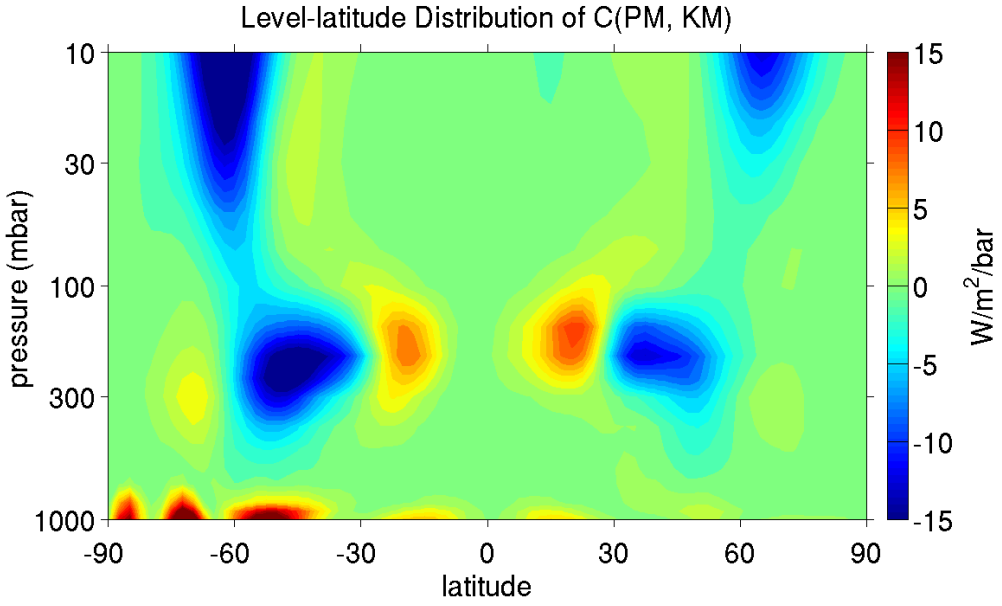

Figure 3.9 Same as Fig. 3.2 except for the conversion rate $C(P_M, K_M)$.

3.4 Summary and Conclusions

This chapter utilizes the 35-year mean states of monthly data from two datasets (NCEP-2 and ERA-Interim) to study the Lorenz energy cycle. Based on two best long-term datasets, our analyses reveal the most-reliable picture of the Lorenz energy cycle for the Earth's global atmosphere. We analyze the spatial mean of four energy components and four conversion rates in Lorenz energy cycle and obtain the structure of Lorenz energy cycle with four types of energies and four conversions with their directions. We also explore the spatial patterns of 35-year mean states of four energy components and find that the structures are consistent with previous results in previous results (Li, Ingersoll et al. 2007, Li, Jiang et al. 2011). These results agree with the atmospheric circulation in the global scales and local storm tracks (Hoskins and Hodges 2005, Ulbrich, Pinto et al. 2008). In addition to the mean available potential energy, mean kinetic energy, eddy potential energy, and eddy kinetic energy, we investigate the spatial patterns of 35-year mean states of four conversion terms. Most of the structures ($C(P_M, P_E)$, $C(K_E, K_M)$, and $C(P_M, K_M)$) are similar with previous results (Li, Ingersoll et al. 2007, Li, Jiang et al. 2011). The only term with noticeable difference is $C(P_E, K_E)$, which shows two bands of centers (one positive, and one negative) on each hemisphere.

4 Temporal Variation of Lorenz Energy Cycle

In this chapter, we will discuss the temporal variation of the Lorenz energy cycle. We already investigated the structure and mean states of the Lorenz energy cycle in Chapter 3. As a very-important part of the atmospheric system, the temporal variation of the Lorenz energy cycle is an important quantity in the dynamic of climate change and global warming. In this chapter, the discussion of the temporal variation of the Lorenz energy cycle is calculated with these two datasets (NCEP-2, and ERA-Interim). The spatial structures (2D, or 3D) of the trends of Lorenz energy cycle will be explored and the spatial patterns of changes of atmospheric energies will be discussed. Then, the deseasonalized and lowpass filtered time series of global averages (weighted average in space) will be calculated. The trends and time series of conversion rates will also be calculated.

4.1 Spatial Structures of Trends of Atmospheric Energies

Atmospheric energies in the Lorenz energy cycle are divided into the mean energies and eddy energies, and the available potential energies and kinetic energies. The behaviors of these different types of energies are related to these different atmospheric phenomena in different scales.

4.1.1 2D Structure of Trend of P_M

Figure 4.1 is a pressure level-latitude distribution of trend of P_M. In this figure, most locations have no significant trends (green areas with trend value around zero). Negative trends are shown in two polar areas near the surface, which indicates the temperature departures from the global average in these areas decrease with time. Since we know that polar areas have a lower temperature compared with the global average temperature. The phenomenon of decreasing polar temperature departures from global average is related to a stronger global warming in these areas than the global average. The two datasets identical the same results in the North Pole region. A different trend appears in South Pole region from the ERA-Interim data. The physics behind the difference in two datasets (NCEP-2, and ERA-Interim) is not clear. Positive trends are

prominent in the mid-stratosphere (30 mbar – 10 mbar) over the two polar regions. This means the temperature at these locations decreased when compared to the global average. The physics supporting this occurrence could be related to depletion of ozone in the polar region in mid-stratosphere, which is much stronger in the Antarctic region than the Arctic region (Farman, Gardiner et al. 1985, Solomon, Garcia et al. 1986, Smith, Prezelin et al. 1992, Randel and Wu 1999).

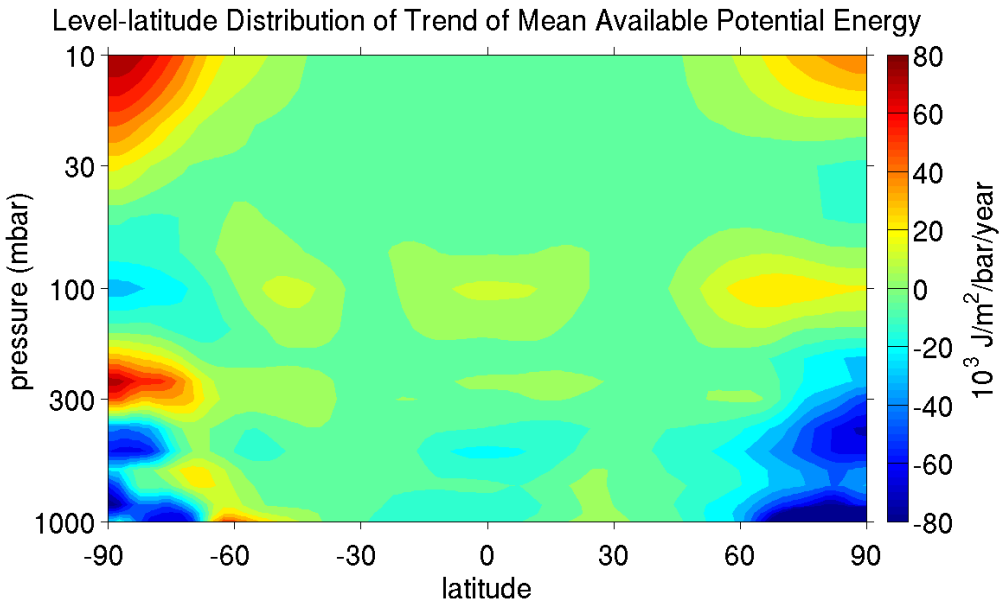

Figure 4.1 Linear trend of mean available potential energy P_M in the pressure-latitude cross-section. The linear trend in each point is calculated over the past 35 years (1979-2013) by least-squares method after filtering the high-frequency signals and ENSO signals.

4.1.2 2D Structure of Trend of K_M

Figure 4.2 is a pressure level-latitude distribution of trend of K_M from the 35-year monthly data. The global mean of K_M did not change considerably during last 35 years. However, there is a positive trend around 60° S in the Southern Hemisphere (SH) and some other trend centers in different locations. The positive trend in the SH could be related to stronger storm tracks, especially over the South Ocean area (Trenberth 1991, Hoskins and Hodges 2005). The zonal asymmetry of storm tracks in the SH (Inatsu and Hoskins 2004) contributes to both mean and eddy kinetic energies. The trend of K_E in the SH will be discussed in Sub-section 4.1.4. The mechanism of positive or negative trend centers of K_M is not clear and more research is needed in the future. Figure 4.2 shows trends of K_M near the surface are approximately zero, which means the large-scale air motion near the surface does not change much.

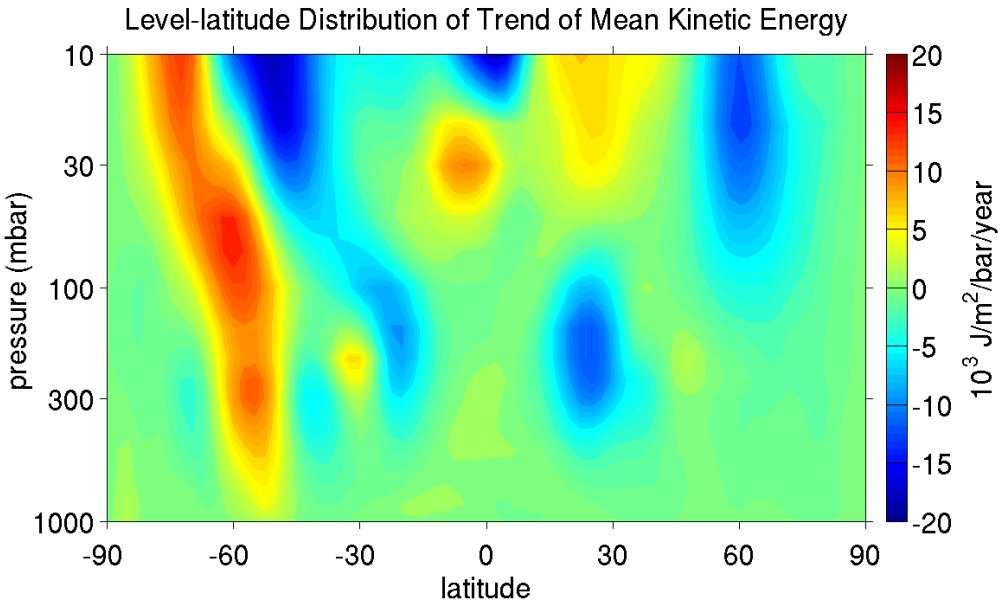

Figure 4.2 Same as Fig. 4.1 except for the mean kinetic energy K_M.

4.1.3 3D Structure of Trend of P_E

Figure 4.3 (a) is pressure level-latitude distribution of trend of P_E. A markedly positive trend is visible in the SH in both the troposphere and stratosphere, which indicates more atmospheric activities over this area. This could also be related to the storm tracks over the Southern Ocean area since storms are usually associated with large P_E. There are two negative trend centers of P_E around 60° to 75° on both hemispheres near the surface. These are related to changes of local atmospheric activities.

Figure 4.3 (b) is the latitude-longitude distribution of trend of P_E from the 35-year monthly data. This map shows a positive trend in the Southern Ocean areas. The trend is not that robust because of a negative trend region near the surface as shown in Figure 4.3 (a). In the NH, a positive trend is located in Northeast Asia and a negative trend in Eastern Canada and Southern Greenland. There are also two negative-trend centers in Tibetan Plateau and Andes Mountain areas, which may be related to climate changes in the high altitude areas.

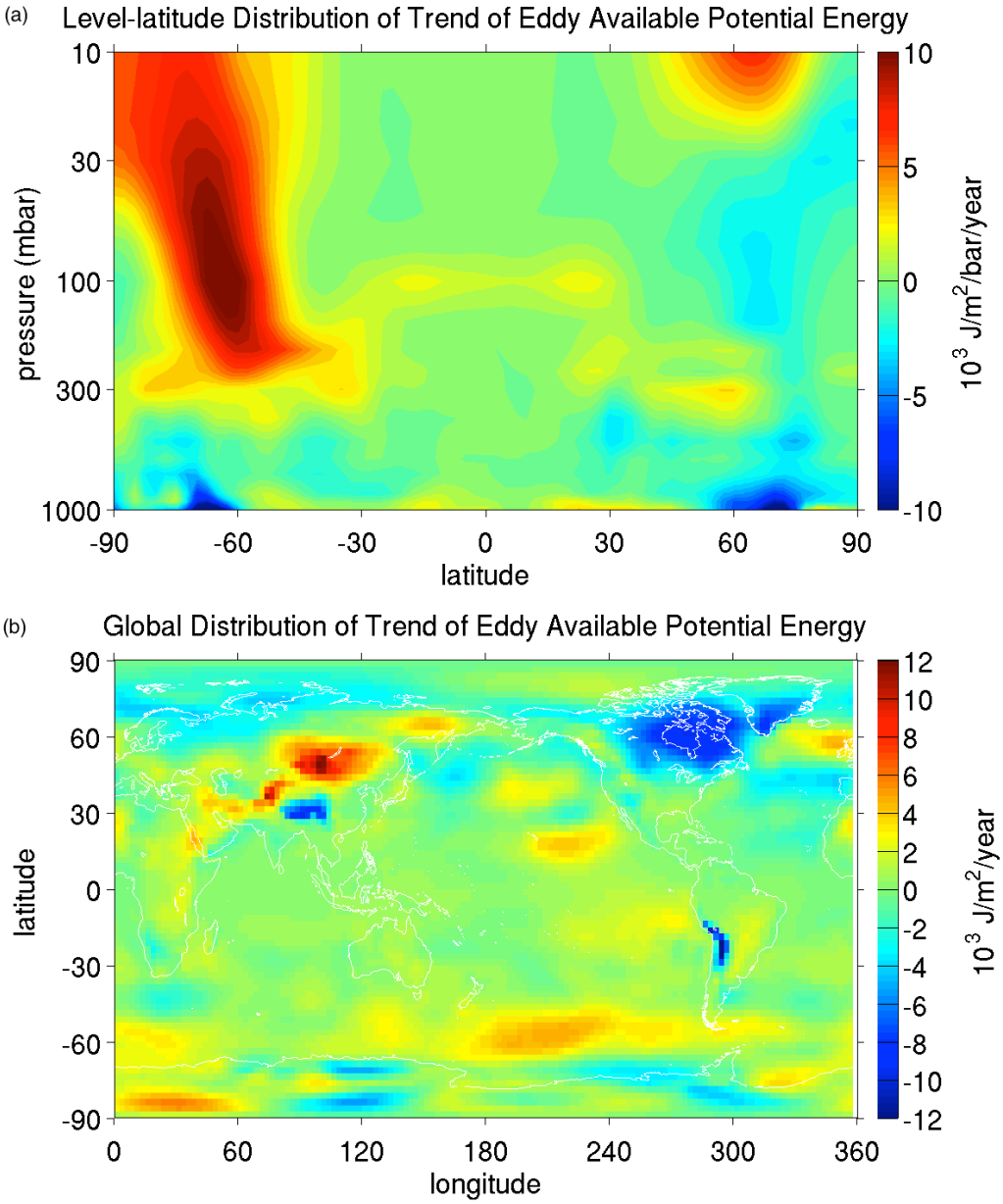

Figure 4.3 Spatial distribution of the linear rend of eddy potential energy P_E. The linear trend in each point is calculated over the past 35 years (1979-2013) by least-squares method after filtering the high-frequency signals and ENSO signals. (a) pressure-latitude cross section, and (b) global distribution in latitude-longitude map. P_E is 3-dimension (pressure-latitude-longitude) structure, so the linear trend of P_E is also 3-dimension structure. The 3-D structure is averaged over one dimension to get the structure in the other 2-dimension cross section.

4.1.4 3D Structure of Trend of K_E

Figure 4.4 (a) is a pressure level-latitude distribution of trend of K_E. A positive trend is shown in the SH and a negative trend in the high latitudes in the NH. These trends are stronger in the mid-stratosphere of the polar regions. A series of positive centers are in the troposphere over the Hadley cell, and the Ferrel cell. The strength of these trend centers decrease from south to north.

Figure 4.4 (b) is a latitude-longitude distribution of trend of K_E. A large-scale positive trend is located over the SH, especially over the Southern Ocean areas. K_E is strongly related to the storm tracks, which indicates that these storm tracks over these areas become stronger. There is also a strong positive trend over the Central Pacific Ocean, which is related to local atmospheric activities. For the NH, there are two negative-trend centers of K_E over the storm tracks in the North Pacific Ocean, and North Atlantic Ocean areas. These trends reflect the changes of storm tracks in these areas.

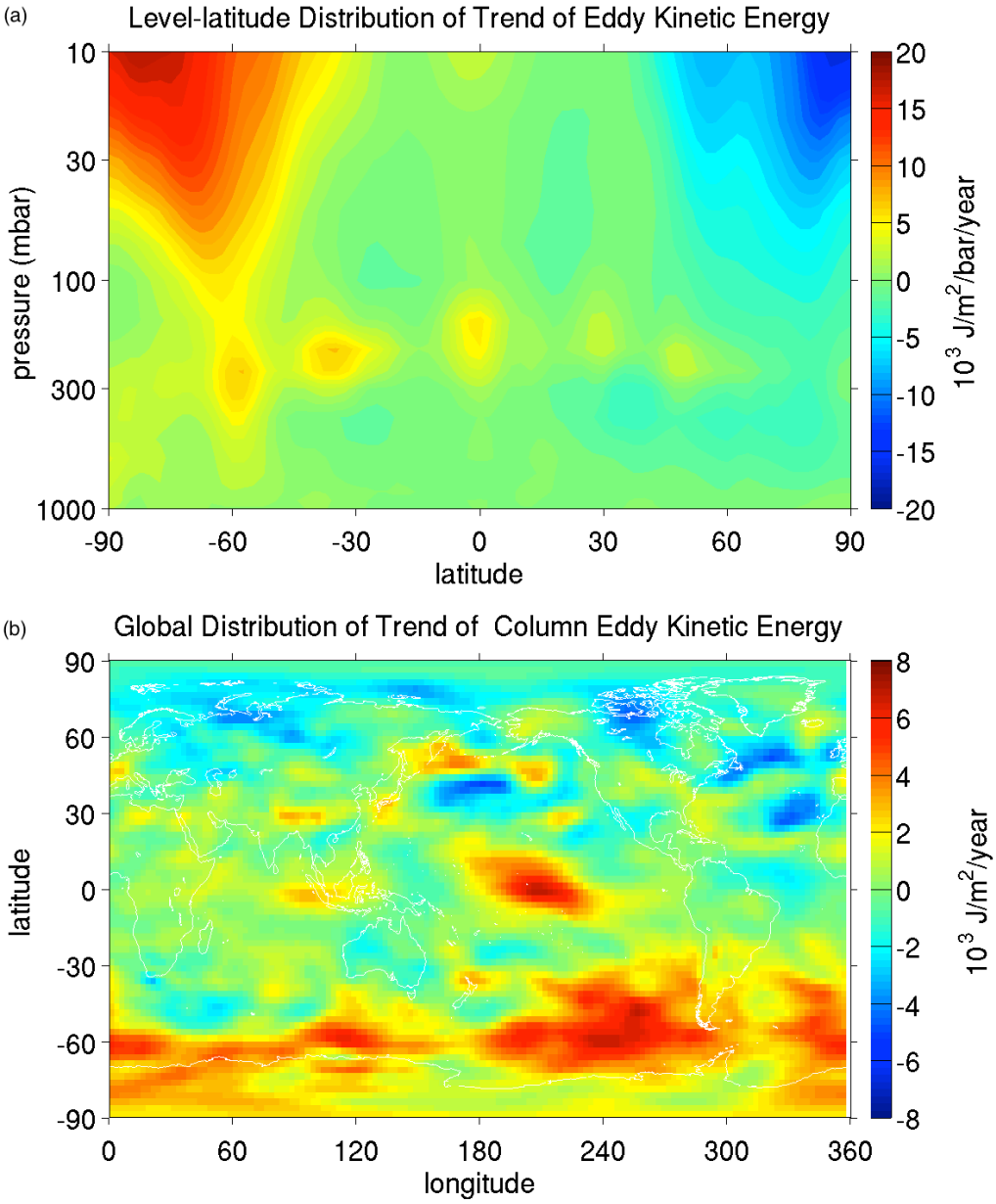

Figure 4.4 Same as Fig. 4.3 except for the eddy kinetic energy K_E.

4.2 Time Series of Atmospheric Energies

In this section, we will explore the time series of the atmospheric energies. We first calculate a weighted (latitude and pressure level) spatial mean of each energy component using the 35-year monthly data. Then we remove the seasonal cycle and high frequency signals from the time series. A lowpass filter is used to remove the high frequency signals in the time series.

This research focuses on the long-term temporal behavior of atmospheric energies with global mean values. To study the changes of atmospheric energies, we apply a linear regression on the time series and calculate a trend with confidence level for each energy component. This would help us obtain a better understanding of the atmospheric energy changes due to global warming and climate change.

4.2.1 Time Series of P_M

Figure 4.5 is a time series of P_M with the 35-year monthly data. The blue solid line is temporal variation of P_M. The red dash line is trend of P_M ($-1.36\pm1.29\times10^3$ J/m^2/year) calculated using the linear regression method. The confidence level with the negative trend is 85.4%. The estimate (using trend with time period) of the change of P_M

during 1979 to 2013 is about -1.09%. This may be related to the stronger warming in the polar regions than global mean.

4.2.2 Time Series of K_M

Figure 4.6 is a time series of K_M with the 35-year monthly data. The blue solid line is temporal variation of K_M. The red dash line is trend of K_M (122±413 J/m^2/year) via the linear regression method. There is no significant change observed in K_M. However, we did find similar low values between K_M and P_M (around year 1981, 1992, and 2003). This suggests that there are possible relationships between K_M and P_M.

4.2.3 Time Series of P_E

Figure 4.7 is a time series of P_E with the 35-year monthly data. The blue solid line is temporal variation of P_E. The red dash line is trend of P_E (346±245 J/m^2/year) via the linear regression method. The confidence level with negative trend is 92.1%. The estimate (using trend with time period) of the change of P_M during 1979 to 2013 is about +2.06%. This may be related to an increasing local (in zonal direction) temperature difference during 1979 to 2013.

4.2.4 Time Series of K_E

Figure 4.8 is a time series of K_E with the 35-year monthly data. The blue solid line is temporal variation of K_E. The red dash line is trend of K_E (645±286 J/m^2/year) via the linear regression method. The confidence level with negative trend is 98.8%. The estimate (using trend with time period) of the change of P_M during 1979 to 2013 is about +3.49%. The increasing trend of K_E is remarkable and the change of K_E during 1979 to 2013 is significant. This may mainly be related to the increased and stronger storms and cyclones during last 35 years (1979-2013).

4.2.5 Time Series of Total Energy ($P_M + K_M + P_E + K_E$)

Figure 4.9 is a time series of total energy ($P_M + K_M + P_E + K_E$) with the 35-year monthly data. The blue solid line is temporal variation of total energy. The red dash line is trend of total energy (-245±1392 J/m^2/year) via the linear regression method. We did not observe a significant trend or change for total atmospheric mechanical energy from the long-term (1979-2013) observations, which suggests that Earth's climate system is still in a quasi-equilibrium state from the energy perspective.

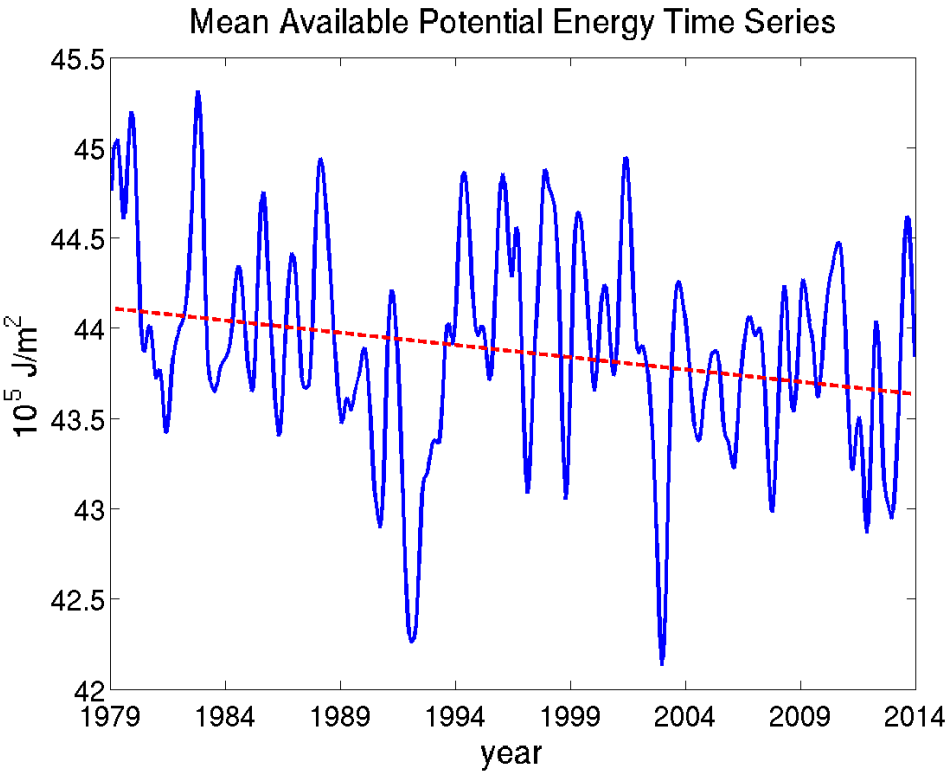

Figure 4.5 Time series of global-average mean available potential energy (P_M) over the past 35 years (1979-2013). The blue solid line is the time series of the monthly data after filtering the seasonal cycle, high- frequency signals, and ENSO signals. The red dash line is the corresponding linear trend using the least-squares method.

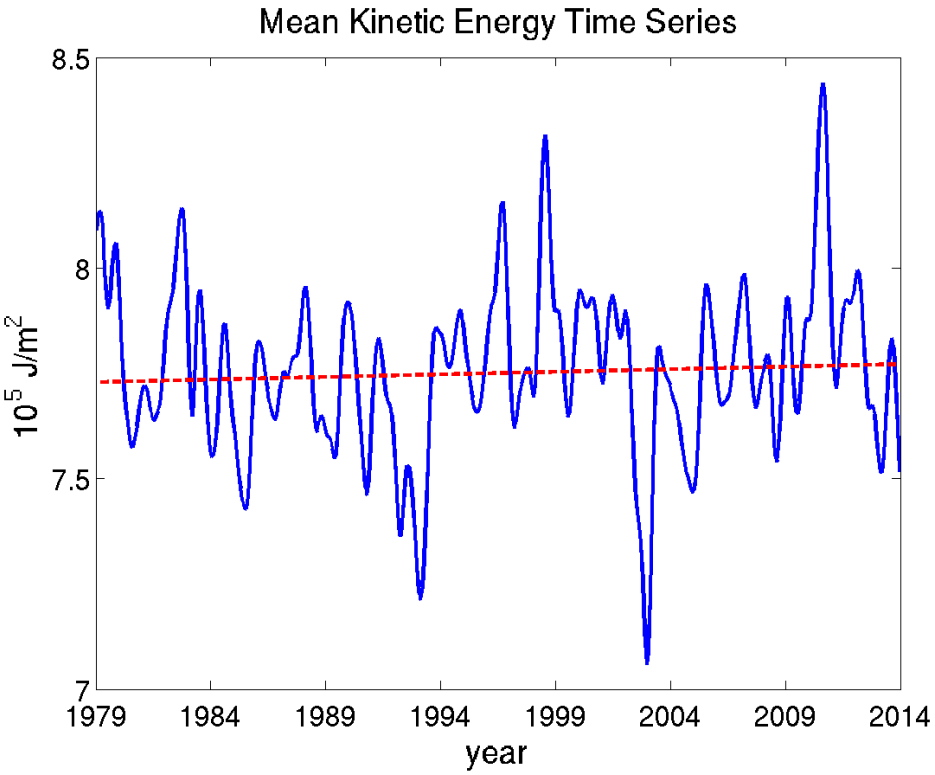

Figure 4.6 Same as Fig. 4.5 except for the mean kinetic energy (K_M).

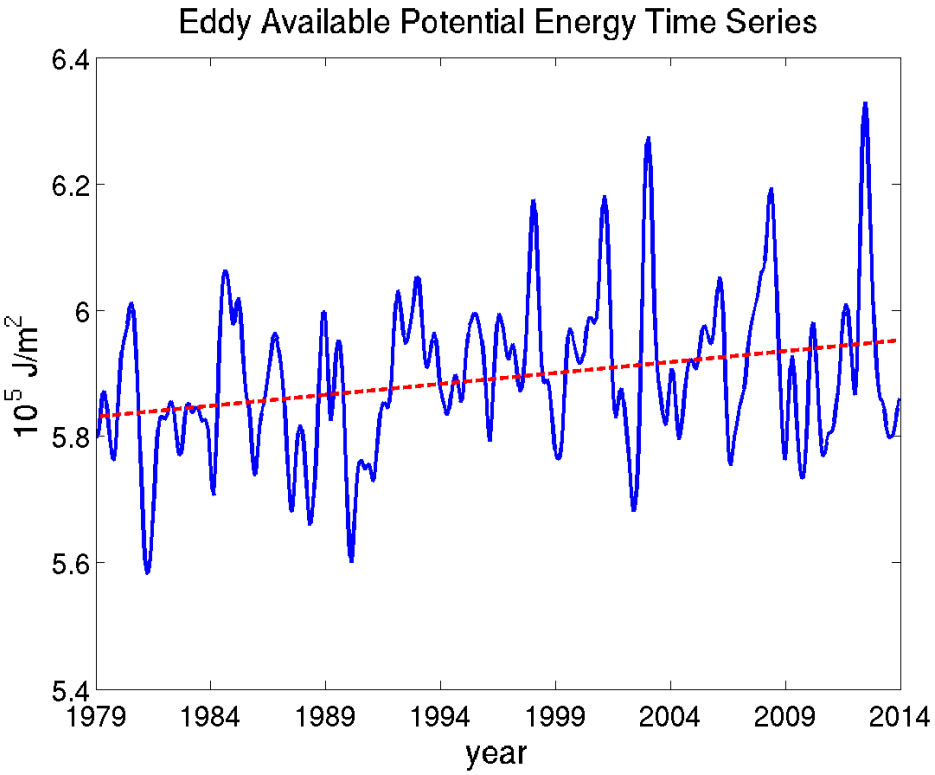

Figure 4.7 Same as Fig. 4.5 except fore the eddy available potential energy (P_E).

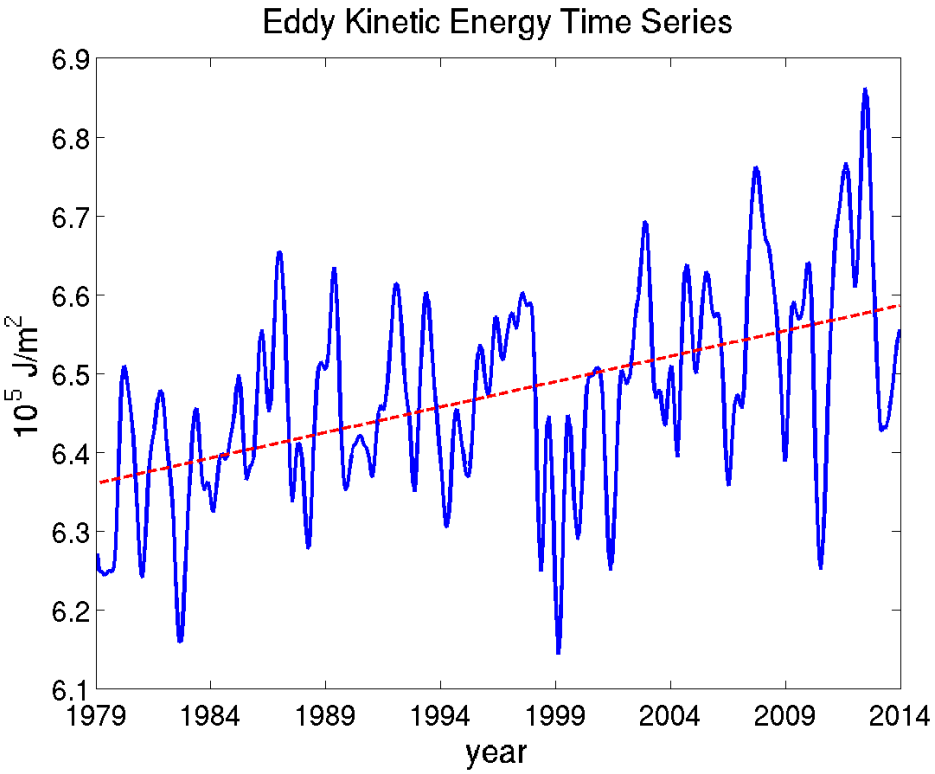

Figure 4.8 Same as Fig. 4.5 except for the eddy kinetic energy (K_E).

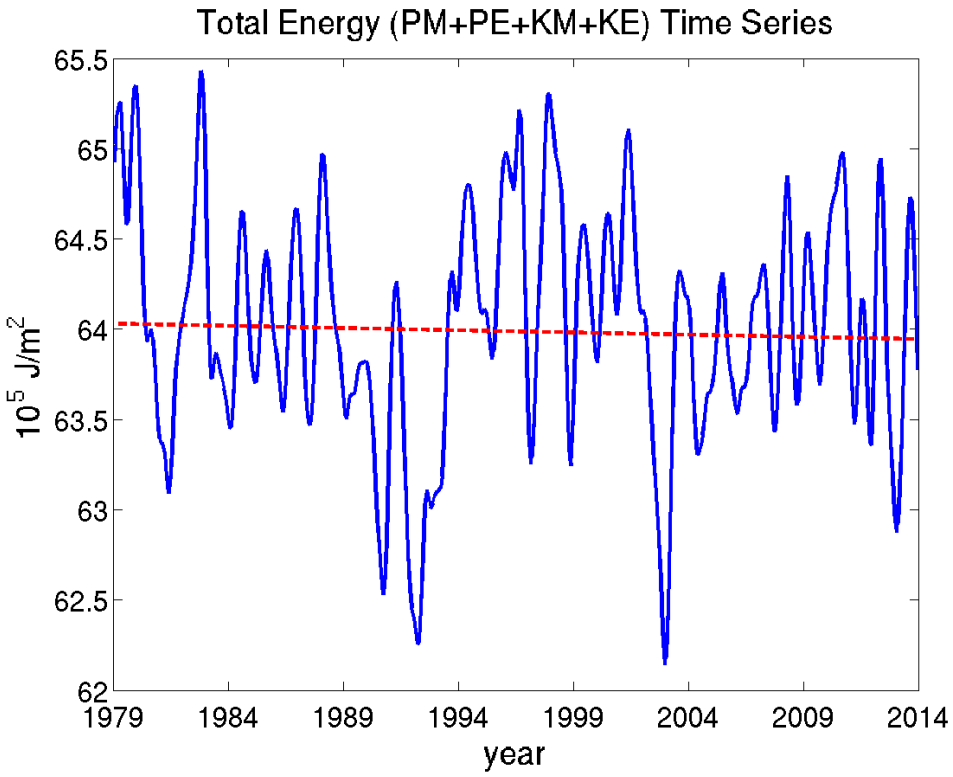

Figure 4.9 Same as Fig. 4.5 except for the total mechanical energy ($P_M + K_M + P_E + K_E$).

4.3 Temporal Variation of Conversion Rates

In this section, the temporal variations of four conversion rates ($C(P_M, P_E)$, $C(P_E, K_E)$, $C(K_E, K_M)$, and $C(P_M, K_M)$) are explored, which connect four energy components (P_M, P_E, K_M, and K_E). The spatial structures (2D or 3D) of trends of the conversion rates are investigated. The temporal variations of conversion rates ($C(P_M, P_E)$, $C(P_E, K_E)$, $C(K_E, K_M)$, and $C(P_M, K_M)$) are very complex and the mechanism is not clear at present. We only show figures of spatial structures and time series with limited discussion in the dissertation. To get a clearer understanding of these figures, future studies are needed.

4.3.1 Temporal Variation of $C(P_M, P_E)$

Figure 4.10 (a) is a pressure level-latitude distribution of trend of $C(P_M, P_E)$. The trends are generally zero at most locations in this figure. Some negative trend centers are near the surface areas. A positive trend is in the mid-troposphere in the SH. A slight negative trend is located in the NH around 60° in the pressure level from 300 mbar to 30

mbar. Figure 4.10 (b) is a time series of global mean of $C(P_M, P_E)$ with the 35-year monthly data. This shows a slight increasing trend during the last 35 years (1979-2013).

4.3.2 Temporal Variation of $C(P_E, K_E)$

Figure 4.11 (a) is a pressure level-latitude distribution of trend of $C(P_E, K_E)$. One positive trend center is in the mid-latitude of the SH in the upper-troposphere (300 mbar-100 mbar). Some band-shaped trend centers of $C(P_E, K_E)$ are in the mid-latitudes of both hemispheres. There are one positive center and one negative center in each hemisphere. The trends (both positive and negative) in the SH are stronger than in the NH, and also a positive trend is located over the South Pole near the surface. Figure 4.11 (b) is a global map of trend of $C(P_E, K_E)$. The trends are only located in the middle and high latitudes and there are almost no trends in the tropical regions (30°S - 30°N). There are positive and negative trends mixed in the middle and high latitudes (30° - 90°) in both hemispheres. This figure also shows that the trends in the SH are stronger than in the NH. Figure 4.12 is a time series of global mean $C(P_E, K_E)$ with the 35-year monthly data. There is no clear trend in the global mean $C(P_E, K_E)$ time series. The conversion rate $C(P_E, K_E)$ between the two eddy energies (P_E and K_E) may not show much information in the global mean data.

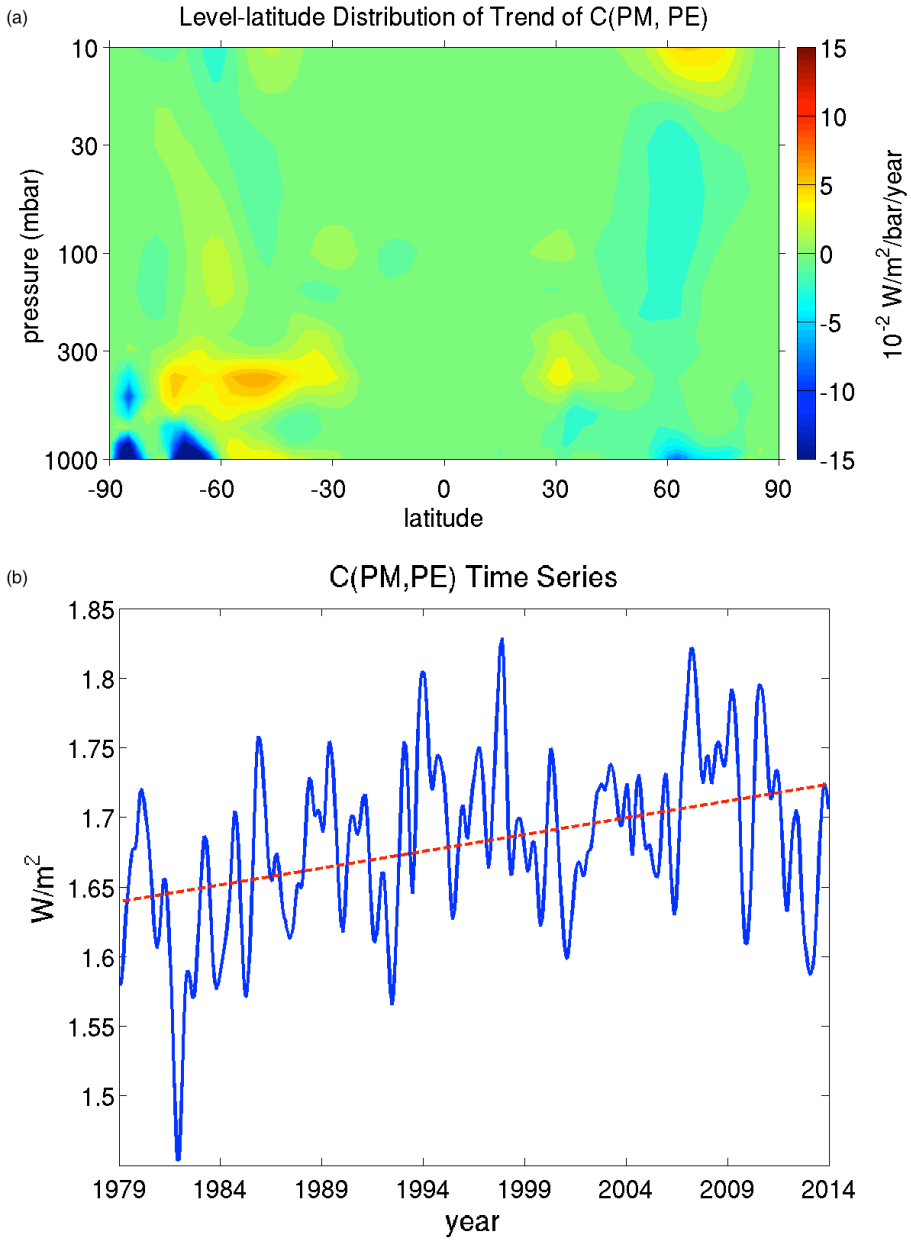

Figure 4.10 Temporal variation of the conversion rate $C(P_M, P_E)$. (a): pressure-latitude cross section of the linear trend, and (b) global-average time series. In panel (a), the linear trend in each point is calculated over the past 35 years (1979-2013) by least-squares method after filtering the high-frequency signals and ENSO signals. In panel (b), the blue solid line is time series of the 35-year monthly data after filtering seasonal cycle, high-frequency signals, and ENSO signals and the red dash line is the corresponding linear trend by a least-squares method.

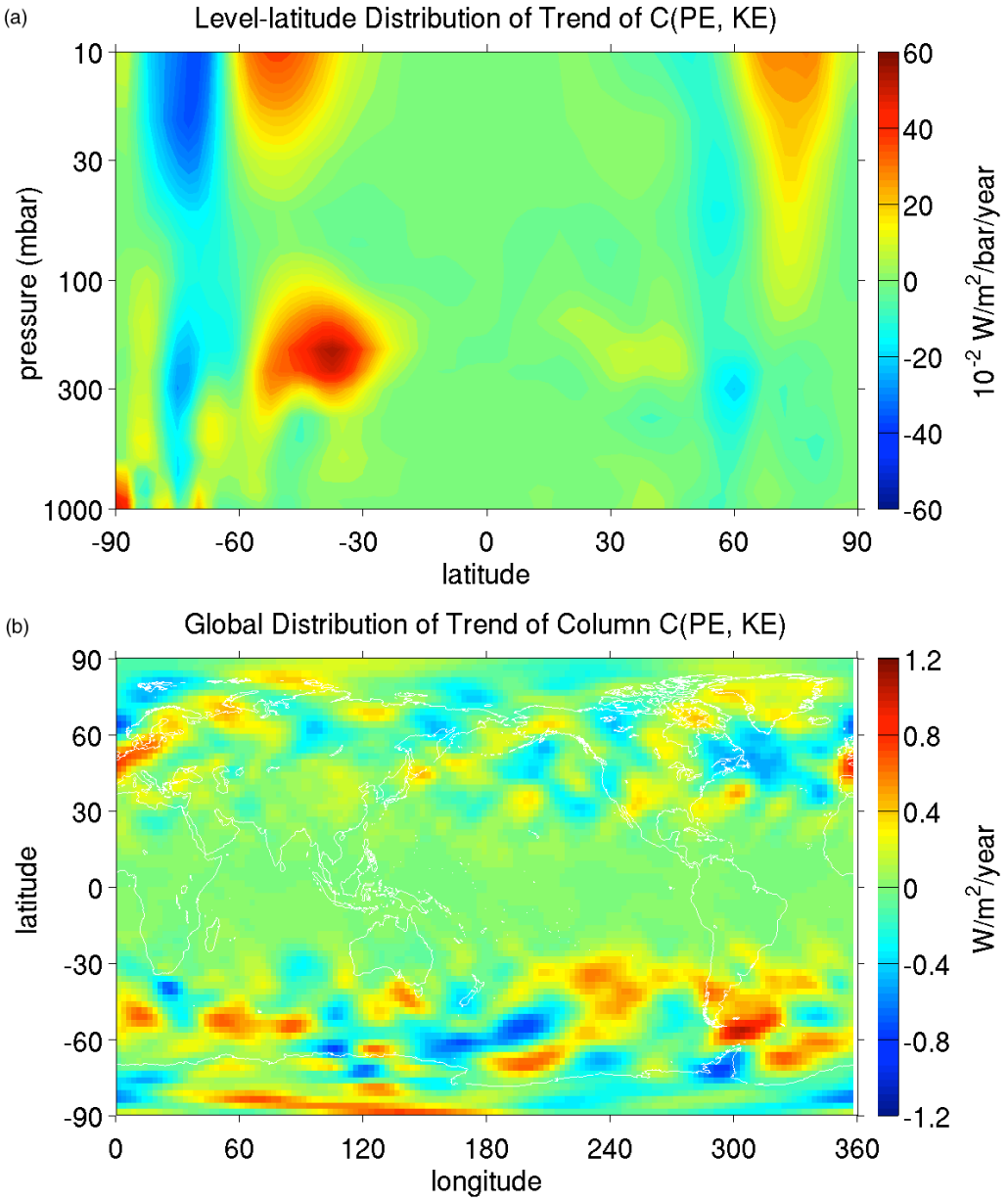

Figure 4.11 Same as Fig. 4.3 except for the conversion rate $C(P_E, K_E)$.

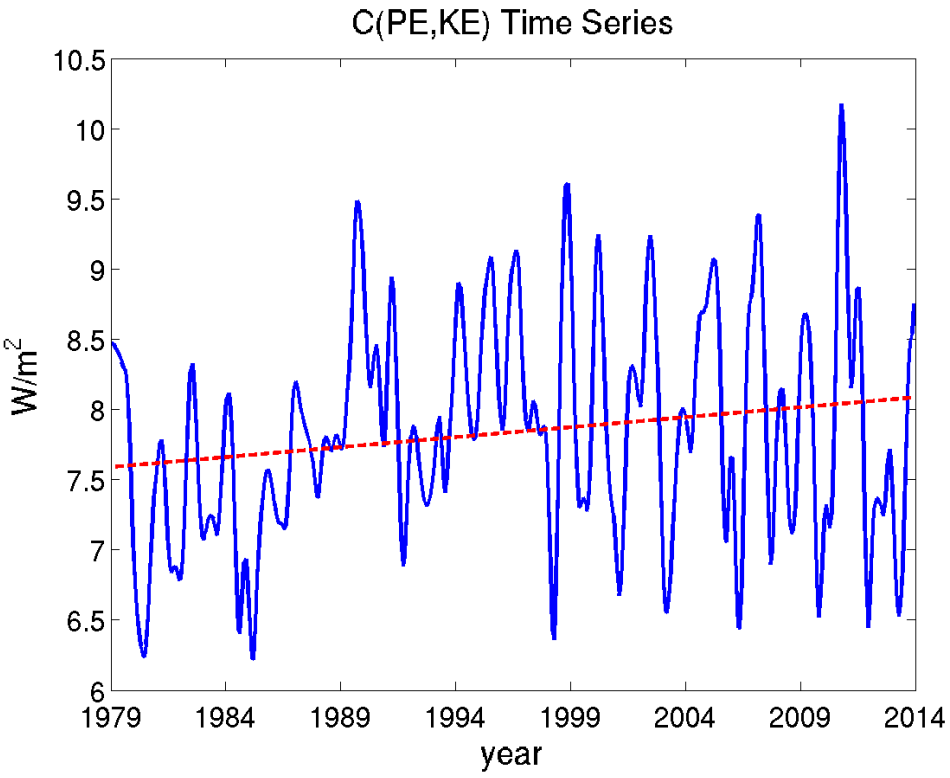

Figure 4.12 (Global-average time series of conversion rate $C(P_E, K_E)$. The blue solid line is time series of the 35-year monthly data after filtering seasonal cycle, high-frequency signals, and ENSO signals and the red dash line is the corresponding linear trend by a least-squares method.

4.3.3 Temporal Variation of $C(K_E, K_M)$

Figure 4.13 (a) is a pressure level-latitude distribution of trend of $C(K_E, K_M)$. There is a positive trend center of $C(K_E, K_M)$ over the South Pole near the surface, and a series of positive negative trend centers of $C(K_E, K_M)$ around 300 mbar pressure level. A strong positive center (15°S - 25°S) and a strong negative center (30°S - 35°S) are in the series of centers in the SH. And we could also get some information that a similar series of centers could be in the 10 mbar pressure level (at the edge of data coverage). Figure 4.13 (b) is a time series global mean of $C(K_E, K_M)$ with the 35-year monthly data. A slight increasing trend is shown in the time series.

4.3.4 Temporal Variation of $C(P_M, K_M)$

Figure 4.14 (a) is a pressure level-latitude distribution of trend of $C(P_M, K_M)$. Three positive trend centers (90°S - 80°S, 75°S - 70°S and 60°S - 45°S) of $C(P_M, K_M)$ are located in the SH near the surface. In the pressure level around 300 mbar, there is one negative trend center (60°S - 45°S) and two positive trend centers (45°S - 25°S and 30°N - 45°N) of $C(P_M, K_M)$, where the trends in the SH (both positive and negative) are much stronger than in the NH. One negative trend center (80°S - 60°S) and one positive trend

center (60°N - 70°N) are located in mid-stratosphere (30 mbar – 10 mbar). Figure 4.14 (b) is a time series global mean of $C(P_M, K_M)$ with the 35-year monthly data. The conversion rate $C(P_M, K_M)$ changed considerably during the last 35-years.

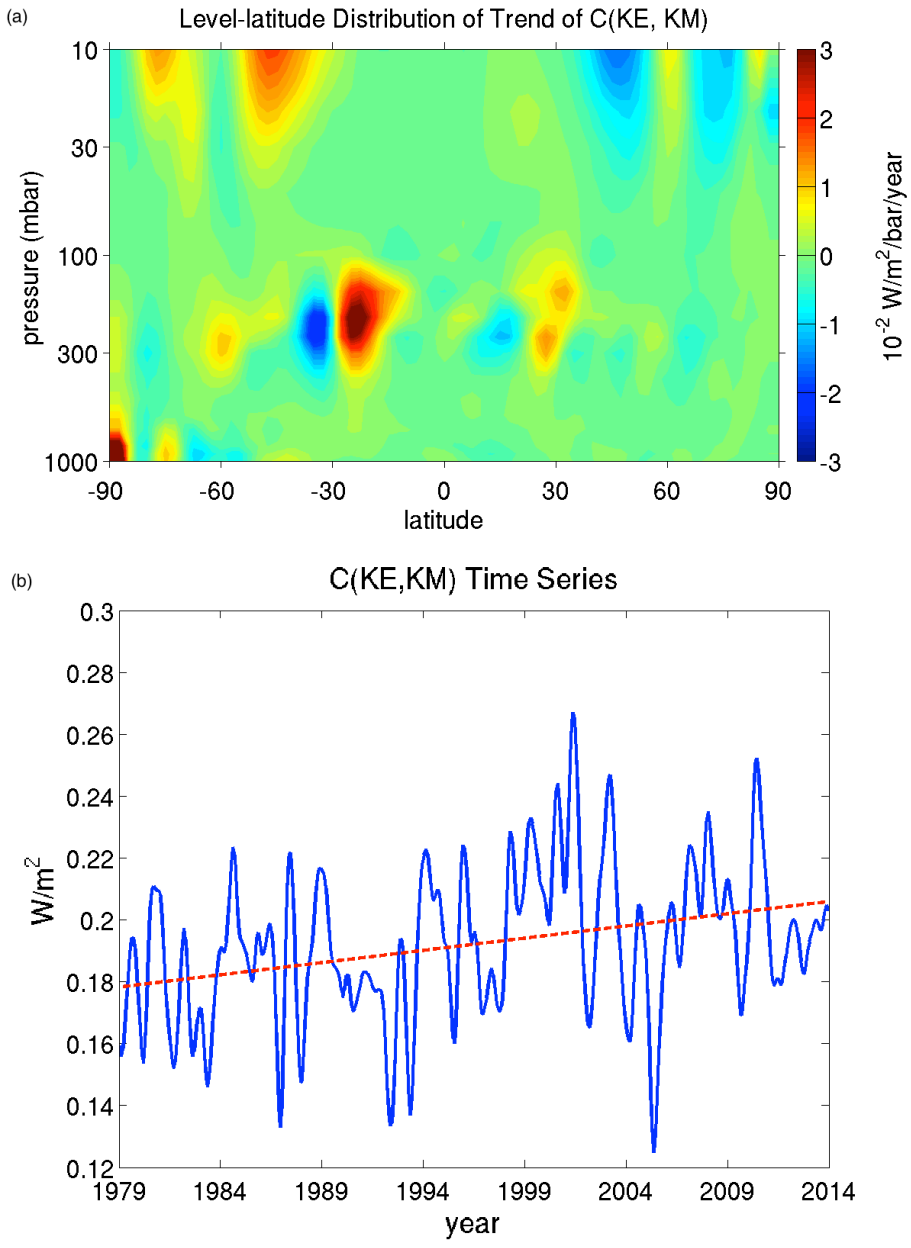

Figure 4.13 Same as Fig. 10 except for the conversion rate $C(K_E, K_M)$.

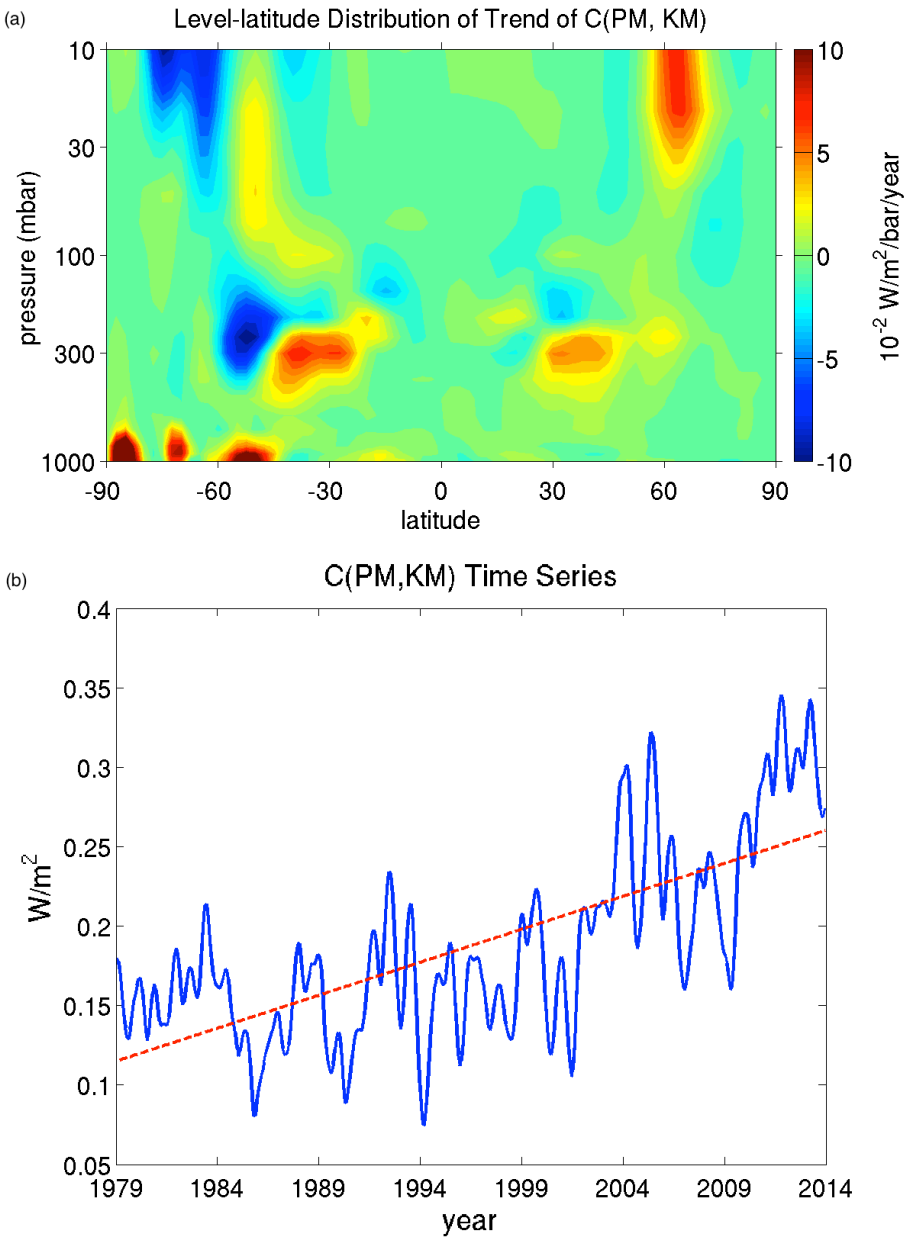

Figure 4.14 Same as Fig. 10 except for the conversion rate $C(P_M, K_M)$.

4.4 Hemispheric Analysis

In the global average time series analysis, three significant trends (positive trend for P_E and K_E, negative trend for P_M) were observed with no significant trends for global average K_M and total mechanical energy. The global average analysis may conceal some features, and more regional or hemispheric analysis may reveal more details about possible trends.

Figure 4.15 is a time series for energy components for NH ((a) – (d)) and SH average ((e) – (h)). In figures 4.15 (a) – (d), which are NH averages, the trends for P_M, P_E, K_M and K_E are -2.63±1.41×10^3 J/m^2/year, 153±297 J/m^2/year, -7±43 J/m^2/year and 7±293 J/m^2/year, respectively. For SH average (figures 4.15 (e) – (h)), the trends for P_M, P_E, K_M, and K_E are 95±1805 J/m^2/year, 706±363 J/m^2/year, 373±703 J/m^2/year and 1.38±0.55×10^3 J/m^2/year, respectively. This reveals that the significant negative trend for global average P_M is mainly in the NH and the significant positive trends for global average P_E and K_E are mainly in the SH. This agrees with the results we got previously in the spatial structures of trend analysis. The negative trend for P_M is mainly located at the North Pole region near the surface and the positive trends for P_E and K_E are mainly located at Southern Ocean storm track areas.

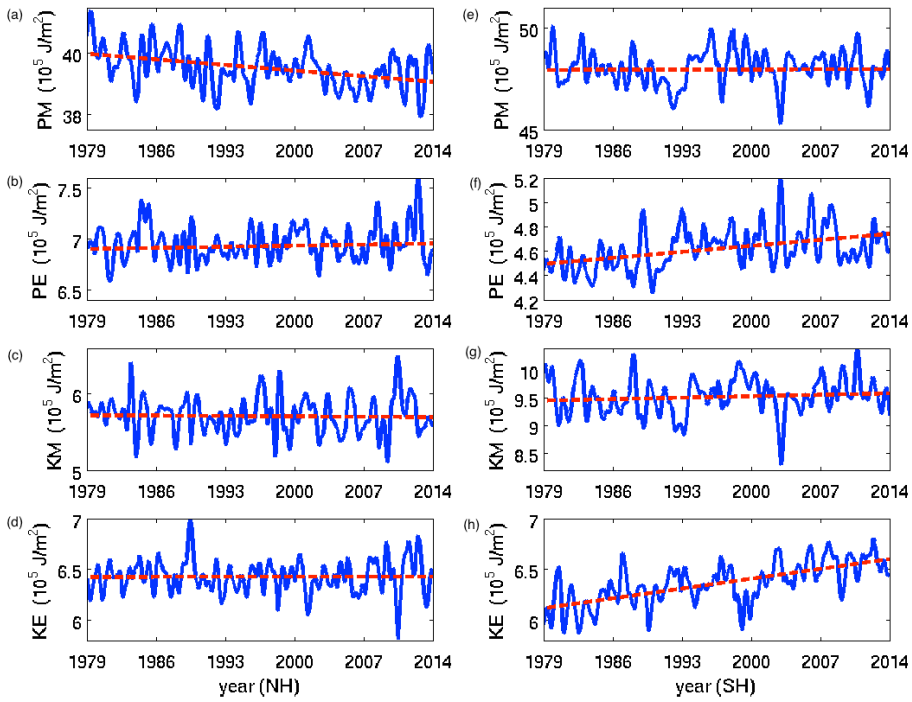

Figure 4.15 Time series of energy components over the two hemispheres (NH and SH) respectively. (a)– (d): time series for P_M, P_E, K_M, and K_E averaging over the NH, and (e) – (h) time series for P_M, P_E, K_M, and K_E averaging over the SH. The blue solid line is time series of the 35-year monthly data after filtering seasonal cycle, high-frequency signals, and ENSO signals and the red dash line is the corresponding linear trend by a least-squares method.

Figure 4.16 is a the time series for total energy ($P_M + K_M + P_E + K_E$) over the NH and SH. Figure 4.16 (a) shows time series for the NH average total energy. There is a significant (94.5%) negative trend (-2.54±1.59 kJ/m^2/year) for the NH average total energy. Figure 4.16 (b) shows time series for the SH average total energy. It illustrates a positive trend (2.56±2.25 kJ/m^2/year) for the SH average total energy.

Both NH and SH show trends for hemispheric average total energy. But these two hemispheric trends (negative for NH and positive for SH) almost cancel each other for the global average, where the global average total energy is not showing a significant trend. The negative trend for NH average total energy is mainly contributed by P_M and the positive trend for SH average total energy is mainly contributed by P_E and K_E.

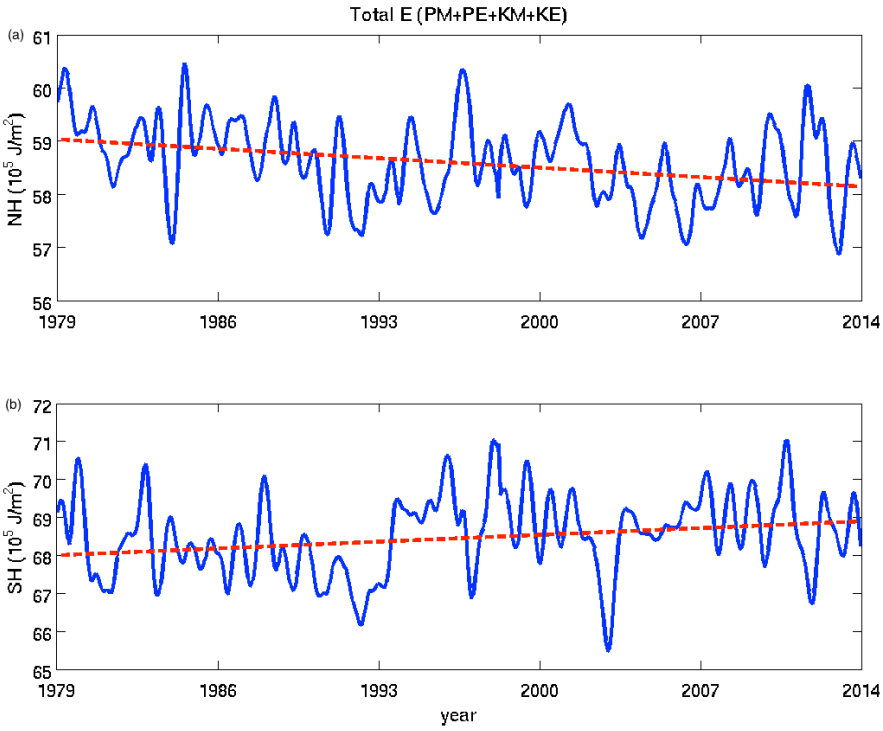

Figure 4.16 Time series of the total mechanical energy ($P_M + K_M + P_E + K_E$) over the two hemispheres (NH and SH) respectively. (a) time series of the total mechanical energy in the NH, and (b) time series of the total mechanical energy in the SH. The blue solid line is time series of the 35-year monthly data after filtering seasonal cycle, high-frequency signals, and ENSO signals and the red dash line is the corresponding linear trend by a least-squares method.

4.5 Summary and Conclusions

In this chapter, the temporal variations of Lorenz energy cycle using the 35-year monthly data from two datasets (NCEP-2 and ERA-Interim) are explored for the first time. Some important characteristics are revealed for the Lorenz energy cycle over the past 35 years. For the time series global mean atmospheric energies (P_M, P_E, K_M, K_E, and Total Energy), some interesting trends with these energy terms were discovered. The negative trend of P_M (-1.36±1.29×10^3 J/m^2/year) may be related to stronger warming in the polar regions than global average. The positive trends of two eddy energies (trend of P_E (346±245 J/m^2/year) and trend of K_E (645±286 J/m^2/year)) may indicate that the atmospheric activities (e.g., temperature perturbation, storms, and cyclones) become more frequent and stronger. The total atmospheric mechanical energy did not show significant change during the last 35 years (1979 – 2013). In the analysis of the spatial structure of trends of atmospheric energies, we found that P_M decreases near the surface of the polar regions, which is associated with stronger warming in these areas. P_M in the mid-stratosphere polar regions (30 mbar – 10 mbar) increases, which is related to the ozone depletion in the mid-stratosphere of the polar regions especially over Antarctica (Farman, Gardiner et al. 1985, Solomon, Garcia et al. 1986, Smith, Prezelin et al. 1992, Randel and Wu 1999). K_E has a strong positive trend in the Southern Ocean and Central Pacific Ocean areas, which is associated with stronger storm activities in these areas. In

the analysis of temporal variation of conversion rates ($C(P_M, P_E)$, $C(P_E, K_E)$, $C(K_E, K_M)$, and $C(P_M, K_M)$), we found that all these conversion rates increased during the last 35 years, which may indicate we have a more efficiency atmospheric system.

5 Conclusions and Discussions

We apply the classical theoretical framework of the Lorenz energy cycle developed by Lorenz (1955) and Oort (1964) to the two best global meteorological datasets from the American National Center for Environmental Prediction/the National Center of Atmospheric Research (NCEP-2) and the European Center for Medium-Range Weather Forecast (EAR-Interim) to compute the Lorenz energy cycle of Earth's global atmosphere. The computed Lorenz energy cycle are further used to examine the mean state and temporal variations of the Lorenz energy cycle of the global atmosphere during the past 35 years (1979-2013). The related physics and applications are also discussed.

First, the mean state of the Lorenz energy cycle of the global atmosphere is updated with the temporal averaging during the past 35 years. Considering that the datasets used in our studies are much better than the datasets used in the previous studies in many aspects (e.g., data quality, spatial coverage, and time period), our analyses provide the most reliable picture of the Lorenz energy cycle. The combination of our analyses and one of our recent studies (Li, Ingersoll et al. 2007) support the classical process of the energy cycle: $P_M \rightarrow P_E \rightarrow K_E \rightarrow K_M$. Our combined results also suggest that the near-surface processes play an important role in the transformations from the mean potential energy to mean kinetic energy, so that the mean kinetic energy P_M is

converted to the mean potential energy K_M in the global scale, which corrects the wrong direction of $C(K_M, P_M)$ presented in the previous studies with the old datasets (Oort 1983). Finally, our new analyses of the mean state of the Lorenz energy cycle provide the most precise value (7.80 W/m^2) for the conversion rate from eddy potential energy to eddy kinetic energy ($C(P_E, K_E)$).

Our analyses of the temporal variations of the Lorenz energy cycle during the past 35 years (1979-2013) also generate some interesting results. A significant negative trend is revealed in the mean available potential energy (P_M) with a value of -1.36±1.29×10^3 J/m^2/year. In addition, strong positive trends are discovered in the two eddy energies (i.e., eddy potential energy P_E and eddy kinetic energy K_E). The analyses of the time series suggest that linear trends ~ 346±245 J/m^2/year and ~ 645±286 J/m^2/year for P_E and K_E, respectively. The spatial structures of the linear trends reveal that the strong positive trends of P_E and K_E and are mainly concentrated in the Southern Ocean and Central Pacific Ocean areas, which are further associated with the intensified storm activities in these areas during the past 35 years. The combined effect of the increased eddy energies (P_E and K_E) and the decreased mean potential energy (P_M) makes the total mechanical energy did not significantly vary during the past 35 years, which suggests that Earth's atmospheric system is still in a quasi-equilibrium state from the energy perspective.

Our analyses further reveal the positive trends in all conversion rates among these energy components, which suggests that the global atmosphere is in a more efficient even though it is still in a quasi-equilibrium state. The increased conversion rates implies the increased dissipation of the kinetic energies, which again suggests that the efficiency of

the atmosphere as a heat engine increased during the past 35 years by following the idea in which the efficiency of atmosphere is defined as the ratio of the dissipation of kinetic energy and the mean incoming solar radiation

The positive trends in the conversion rates among different energies suggest that the significant changes exist in the generation and dissipation terms of the Lorenz energy cycle. These changes in the generation and dissipation terms suggested by the conversion terms offer important hints to the distribution and variability on the global and local heating (cooling), and friction and turbulence associated with mean and eddy circulations, which can not be measured easily. These temporal characteristics of the conversion rates and the corresponding energy components provide one more perspective to understand, monitor, and predict the climate changes on Earth. These characteristics also play important roles in validating and developing climate models because they constitute the constraints that must be fulfilled.

Appendix 1 Structure of Atmosphere

Our Earth is covered by thousands of miles of atmosphere. Air pressure and density decrease with altitude in the atmosphere. But air temperature is more complicated in the altitude. Usually, the atmosphere above 700 km (440 miles) is defined as exosphere, which is the outermost layer of Earth's atmosphere. There are only extremely low densities of hydrogen, helium and several other molecules. The atoms and molecules are far apart and the behavior of exosphere is no longer like a gas. Below exosphere, there are four layers of atmosphere defined by the temperature behavior in altitudes.

These four layers (thermosphere, mesosphere, stratosphere and troposphere) are divided by three boundaries (mesopause, stratopause and tropopause) with behaviors of temperatures in these layers (Figure A1).

Thermosphere is the top layer of these four layers. The altitude is 80 to 700 km (50 to 440 miles). Temperature is decreasing when altitude is increasing in this layer. This phenomenon is because this layer contains the ionosphere (lots of ions), which could absorb solar radiation directly. This could result the higher altitude has higher temperature. Mesosphere is the next layer between stratopause and mesopause. The altitude is 50 to 80 km (31 to 50 miles). Temperature is increasing when altitude increases in this layer. Stratosphere is the third layer in these four layers, which is 12 to 50 km (7 to 31 miles). Temperature in stratosphere behaves like thermosphere:

temperature increases while altitude increases. The reason is this layer contains ozone layer, which could absorb ultraviolet radiation (UV) from the Sun. The last or the lowest layer of Earth's atmosphere is troposphere. The altitude is 0 to 12 km (0 to 7 miles). Temperature decreases while altitude increases in this layer. This layer contains the weather layer.

In this dissertation, we are computing atmospheric energies from surface to 10-mbar-pressure level (or around 30 km), which is the total troposphere and lower stratosphere. Almost 99% of energies are contained in these layers.

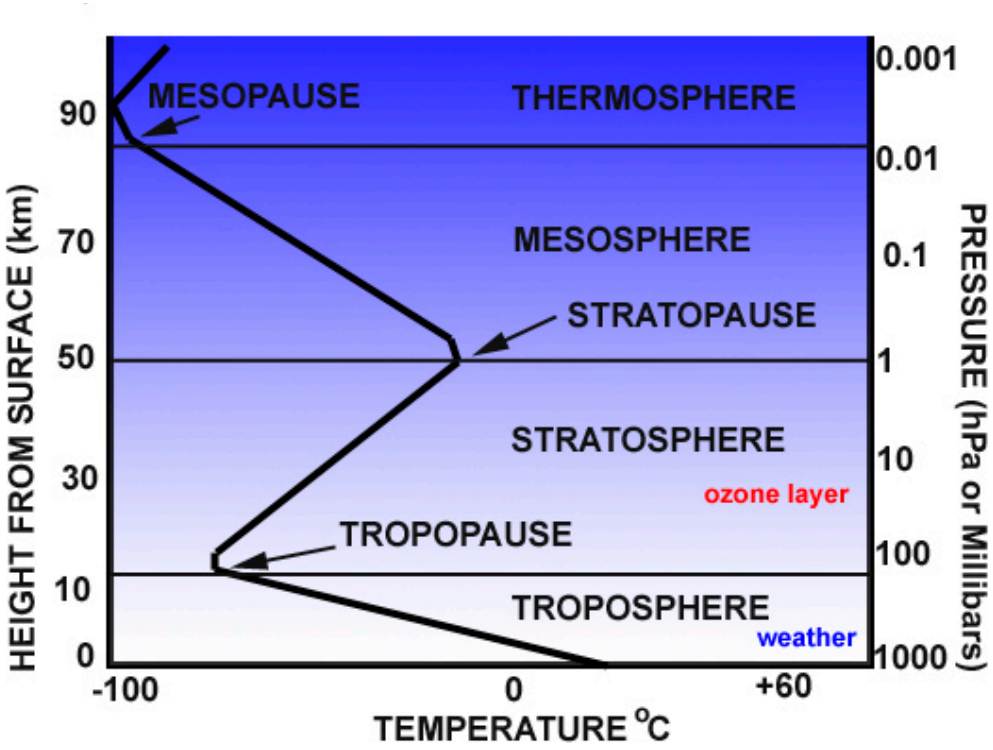

Figure A1 Four layers of Earth's atmosphere

Appendix 2 Atmospheric circulation

Atmospheric circulation is the large-scale movement of air, which is driven by thermal energy (e.g., available potential energy) on the surface of the Earth. The large-scale structure of atmospheric circulation drifts by seasons and varies by years. But the basic structure remains fairly constant. The most important circulation is circulation in the latitude direction with three cells (Hadley cell, Ferrel cell and Polar cell). Figure A2 shows a simplified model of the three cells. This figure shows the average positions of these cells. However, the circulation cells are moving by seasons with temperature distribution and the boundaries of cells are not exactly on latitude circles, which are affected by surface of earth (e.g., oceans, lands).

Hadley cell

George Hadley first described Hadley cell in the early 18th century and the theory was widely accepted in the 19th century. The mechanism of Hadley cell is thermo driven circulation. The atmosphere near equator is receiving most solar heat and rising up, then moving to higher latitudes near the tropopause, sinking in the subtropics (around 30°N and 30°S), finally returning back to equator in the near surface. The winds are not exact in the meridional direction since they are affected by the Coriolis effect, which turns

winds to the right in the Northern Hemisphere and to the left in the Southern Hemisphere. These result the subtropical jet streams and trade winds. The center of Hadley cell, or Intertropical Convergence Zone (ITCZ) moves to the Northern Hemisphere in July and to the Southern Hemisphere in Januagy.

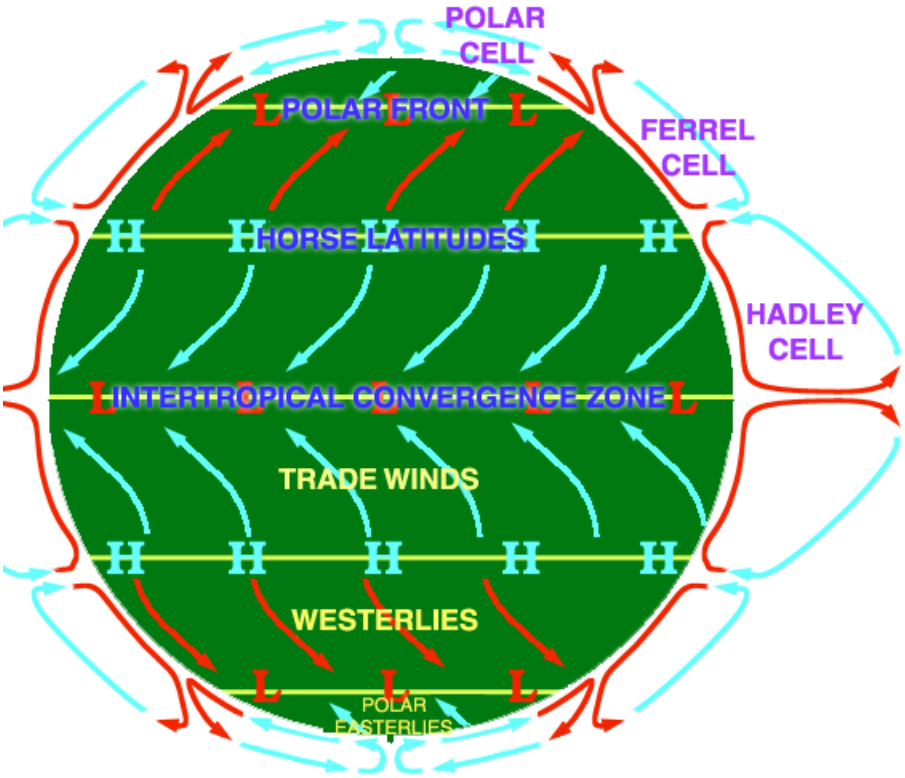

Figure A2 Atmospheric circulation (three cells)

Polar cell

Polar cell is also a thermo driven cell with a similar mechanism like Hadley cell. The circulation in Polar cell is limited in high latitudes (over 60°N or 60°S) in the troposphere (tropopause in Polar Regions is about 8 km). The air rises in lower latitudes (60°N or 60°S) and moves poleward in the upper troposphere at both North and South Poles. And the cooled air reaches the polar areas, sinks and moves back to the low latitudes in the near surface. Polar cell is also affected by the Coriolis effect, which results the Polar easterlies.

Ferrel cell

Ferrel cell is not a thermo driven cell and is a secondary circulation driven by the motion, which behaves as an atmospheric ball bearing between Hadley cell and Polar cell. In the Ferrel cell, air rises around 60° (N or S) near Polar cell and moves towards to lower latitudes (30°N or 30°S), then sinks near Hadley cell and moves back to higher latitudes (60°N or 60°S) in the near surface. The wind in the near surface affected by the Coriolis effect is referred to as the Westerlies.

There are also some circulations in the longitude direction. One large circulation in the longitude direction is Walker circulation, which is related to El Niño – Southern

Oscillation (ENSO). We are not talking much about this circulation much in this dissertation.

References

Dee, D. P., S. M. Uppala, A. J. Simmons, P. Berrisford, P. Poli, S. Kobayashi, U. Andrae, M. A. Balmaseda, G. Balsamo, P. Bauer, P. Bechtold, A. C. M. Beljaars, L. van de Berg, J. Bidlot, N. Bormann, C. Delsol, R. Dragani, M. Fuentes, A. J. Geer, L. Haimberger, S. B. Healy, H. Hersbach, E. V. Holm, L. Isaksen, P. Kallberg, M. Kohler, M. Matricardi, A. P. McNally, B. M. Monge-Sanz, J. J. Morcrette, B. K. Park, C. Peubey, P. de Rosnay, C. Tavolato, J. N. Thepaut and F. Vitart (2011). "The ERA-Interim reanalysis: configuration and performance of the data assimilation system." Quarterly Journal of the Royal Meteorological Society **137**(656): 553-597.

Farman, J. C., B. G. Gardiner and J. D. Shanklin (1985). "Large Losses of Total Ozone in Antarctica Reveal Seasonal Clox/Nox Interaction." Nature **315**(6016): 207-210.

Hartmann, D. L. (1994). Global physical climatology. San Diego, Academic Press.

Hoskins, B. J. and K. I. Hodges (2005). "A new perspective on Southern Hemisphere storm tracks." Journal of Climate **18**(20): 4108-4129.

Hu, Q., Y. Tawaye and S. Feng (2004). "Variations of the Northern Hemisphere atmospheric energetics: 1948-2000." Journal of Climate **17**(10): 1975-1986.

Inatsu, M. and B. J. Hoskins (2004). "The zonal asymmetry of the Southern Hemisphere winter storm track." Journal of Climate **17**(24): 4882-4892.

Kalnay, E., M. Kanamitsu, R. Kistler, W. Collins, D. Deaven, L. Gandin, M. Iredell, S. Saha, G. White, J. Woollen, Y. Zhu, M. Chelliah, W. Ebisuzaki, W. Higgins, J.

Janowiak, K. C. Mo, C. Ropelewski, J. Wang, A. Leetmaa, R. Reynolds, R. Jenne and D. Joseph (1996). "The NCEP/NCAR 40-year reanalysis project." Bulletin of the American Meteorological Society **77**(3): 437-471.

Kanamitsu, M., W. Ebisuzaki, J. Woollen, S. K. Yang, J. J. Hnilo, M. Fiorino and G. L. Potter (2002). "NCEP-DOE AMIP-II reanalysis (R-2)." Bulletin of the American Meteorological Society **83**(11): 1631-1643.

Krueger, A. F., J. S. Winston and D. A. Haines (1965). "Computation of atmospheric energy and its transformation for the Northern Hemisphere for a recent five-year period." Mon. Wea. Rev **93**: 227-238.

Li, L. M., A. P. Ingersoll, X. Jiang, D. Feldman and Y. L. Yung (2007). "Lorenz energy cycle of the global atmosphere based on reanalysis datasets." Geophysical Research Letters **34**(16).

Li, L. M., X. Jiang, M. T. Chahine, J. Q. Wang and Y. L. Yung (2011). "The Mechanical Energies of the Global Atmosphere in El Nino and La Nina Years." Journal of the Atmospheric Sciences **68**(12): 3072-3078.

Lorenz, E. N. (1955). "Available Potential Energy and the Maintenance of the General Circulation." Tellus **7**(2): 157-167.

Margules, M. (1903). "Uber die energie der stiirme." Jahrb. kais.-kon. Zent. fur Met., Vienna. Translation by C. Abbe in Smithson. Misc. Coll **51**: 1910.

Oort, A. H. (1964). "On the Energetics of the Mean and Eddy Circulations in the Lower Stratosphere." Tellus **16**(3): 309-327.

Oort, A. H. (1983). Global atmospheric circulation statistics, 1958-1973, US Department of Commerce, National Oceanic and Atmospheric Administration.

Oort, A. H. and J. P. Peixoto (1974). "Annual Cycle of Energetics of Atmosphere on a Planetary Scale." Journal of Geophysical Research **79**(18): 2705-2719.

Oort, A. H. and J. P. Peixoto (1976). "Variability of Atmospheric Energy Cycle within a 5-Year Period." Journal of Geophysical Research-Oceans and Atmospheres **81**(21): 3643-3659.

Peixoto, J. P. and A. H. Oort (1974). "Annual Distribution of Atmospheric Energy on a Planetary Scale." Journal of Geophysical Research **79**(15): 2149-2159.

Peixoto, J. P. and A. H. Oort (1992). Physics of climate. New York, American Institute of Physics.

Phillips, N. A. (1956). "The General Circulation of the Atmosphere - a Numerical Experiment." Quarterly Journal of the Royal Meteorological Society **82**(352): 123-164.

Randel, W. J. and F. Wu (1999). "Cooling of the arctic and antarctic polar stratospheres due to ozone depletion." Journal of Climate **12**(5): 1467-1479.

Saltzman, B. (1957). "Equations Governing the Energetics of the Larger Scales of Atmospheric Turbulence in the Domain of Wave Number." Journal of Meteorology **14**(6): 513-523.

Sheng, J. and Y. Hayashi (1990). "Observed and Simulated Energy Cycles in the Frequency-Domain." Journal of the Atmospheric Sciences **47**(10): 1243-1254.

Smith, R. C., B. B. Prezelin, K. S. Baker, R. R. Bidigare, N. P. Boucher, T. Coley, D. Karentz, S. Macintyre, H. A. Matlick, D. Menzies, M. Ondrusek, Z. Wan and K. J. Waters (1992). "Ozone Depletion - Ultraviolet-Radiation and Phytoplankton Biology in Antarctic Waters." Science **255**(5047): 952-959.

Solomon, S., R. R. Garcia, F. S. Rowland and D. J. Wuebbles (1986). "On the Depletion of Antarctic Ozone." Nature **321**(6072): 755-758.

Trenberth, K. E. (1991). "Storm Tracks in the Southern-Hemisphere." Journal of the Atmospheric Sciences **48**(19): 2159-2178.

Ulbrich, U., J. G. Pinto, H. Kupfer, G. C. Leckebusch, T. Spangehl and M. Reyers (2008). "Changing northern hemisphere storm tracks in an ensemble of IPCC climate change simulations." Journal of Climate **21**(8): 1669-1679.

Uppala, S. (2002). "ECMWF reanalysis, 1957–2001, ERA-40." ERA-40 Project Report Series **3**: 1-10.

Uppala, S. M., P. W. Kallberg, A. J. Simmons, U. Andrae, V. D. Bechtold, M. Fiorino, J. K. Gibson, J. Haseler, A. Hernandez, G. A. Kelly, X. Li, K. Onogi, S. Saarinen, N. Sokka, R. P. Allan, E. Andersson, K. Arpe, M. A. Balmaseda, A. C. M. Beljaars, L. Van De Berg, J. Bidlot, N. Bormann, S. Caires, F. Chevallier, A. Dethof, M. Dragosavac, M. Fisher, M. Fuentes, S. Hagemann, E. Holm, B. J. Hoskins, L. Isaksen, P. A. E. M. Janssen, R. Jenne, A. P. McNally, J. F. Mahfouf, J. J. Morcrette, N. A. Rayner, R. W. Saunders, P. Simon, A. Sterl, K. E. Trenberth, A. Untch, D. Vasiljevic, P. Viterbo and J. Woollen (2005). "The ERA-40 re-analysis." Quarterly Journal of the Royal Meteorological Society **131**(612): 2961-3012.

Wiinniel.A, Steinber.L and M. Drake (1967). "Maintenance of Temperature Amplitude in Atmosphere." Journal of Geophysical Research **72**(2): 461-&.